

# Structure and properties of small sodium clusters.

Ilia A Solov'yov<sup>†</sup>, Andrey V Solov'yov<sup>‡</sup> and Walter Greiner<sup>§</sup>

Institut für Theoretische Physik der Johann Wolfgang Goethe-Universität, 60054  
Frankfurt am Main, Germany

**Abstract.** We have investigated structure and properties of small metal clusters using all-electron *ab initio* theoretical methods based on the Hartree-Fock approximation and density functional theory, perturbation theory and compared results of our calculations with the available experimental data and the results of other theoretical works. We have systematically calculated the optimized geometries of neutral and singly charged sodium clusters having up to 20 atoms, their multipole moments (dipole and quadrupole), static polarizabilities, binding energies per atom, ionization potentials and frequencies of normal vibration modes. Our calculations demonstrate the great role of many-electron correlations in the formation of electronic and ionic structure of small metal clusters and form a good basis for further detailed study of their dynamic properties, as well as structure and properties of other atomic cluster systems.

## 1. Introduction

Atomic clusters and small nanoparticles have been recognized as new physical objects with their own properties relatively recently. This became clear after such experimental successes as the discovery of electron shell structure in metal clusters [1], observation of plasmon resonances in metal clusters [2–4] and fullerenes [5, 6], formation of singly and doubly charged negative cluster ions [7] and many more others. The novelty of cluster physics is also greatly connected with the fact that cluster properties explain the transition from single atoms or molecules to solid state. Comprehensive survey of the field can be found in review papers and books, see e.g. [8–14].

There are many different types of clusters, such as metallic clusters, fullerenes, molecular clusters, semiconductor clusters, organic clusters, quantum dots, positively and negatively charged clusters, which all have their own features and properties. In this paper we focus on the detailed systematic study of the structure and properties of small metal clusters and in particular sodium clusters using *ab initio* all-electron many-body theory methods.

<sup>†</sup> E-mail: solovyov@rpro.ioffe.rssi.ru; on leave from St.Petersburg State Technical University, Politechnicheskaya 29, 195251 St.Petersburg, Russia

<sup>‡</sup> E-mail: solovyov@th.physik.uni-frankfurt.de; on leave from A.F.Ioffe Physical-Technical Institute, Russian Academy of Sciences, Politechnicheskaya 26, St. Petersburg 194021, Russia

<sup>§</sup> E-mail: greiner@th.physik.uni-frankfurt.de

So far, for sodium clusters, systematic calculations of cluster properties on the same level of theory as in our present work (i.e. all electron *ab initio*) have been performed only for clusters with  $N \leq 10$  [13, 15–19], where  $N$  is a number of atoms in a cluster. In our work we extend this limit up to  $N \leq 20$ . Note that most of the cited papers are focused on the investigation of neutral cluster properties rather than ions. In our present work we perform systematic comparative analysis of properties of neutral and singly charged sodium clusters in the specified size range.

During the last decade, there were performed numerous experimental and theoretical investigations of the properties of small metal clusters as well as the processes with their involvement. Here we are not able to review even all essential results obtained in the field and only refer to those, which are related the most closely to the subject of our paper. In [1], it was experimentally proved that metal clusters have the shell electronic structure and the magic cluster numbers have been determined by observation of the sodium cluster abundances in mass spectra. Experimental study of electronic structure and properties of small metal clusters have been performed in [20, 21] (for review also see [8, 10, 11, 13, 14]). In [20], there have been measured the ionisation potentials for a sequence of small neutral and positively charged sodium metal clusters, which independently proved their shell structure. The dipole polarizabilities of sodium clusters have been experimentally determined in [21]. Dissociation energies of neutral and positively charged small sodium and potassium metal clusters have been measured in [22–24]. Dynamical properties of clusters have been studied by means of photon, electron and ion scattering. These methods are the traditional tools for probing properties and internal structure of various physical objects. Using these methods, for example, plasmon excitations in metal clusters [2, 25] and fullerenes [6] have been observed (for review also see [8, 10]).

Metal clusters have also been studied theoretically. Structural properties of small metal clusters have been widely investigated using quantum chemistry methods. Here we refer to the papers [15–18, 26–29], in which optimized geometries, binding energies, ionization potentials, electron structure and electron transport properties of small lithium and sodium clusters have been calculated. In these papers the systematic analysis of the cluster properties has been limited by cluster sizes  $N \leq 10$ . In the present paper we extend this limit up to  $N \leq 20$  and perform systematic analysis of various cluster characteristics both for neutral clusters and singly charged cluster ions.

In a last few years, a number of papers have been devoted to the calculation of dipole static polarizabilities of neutral sodium and lithium clusters [19, 30–33]. Note that most of these studies have been performed within the cluster size range  $N \leq 20$ . The results of different theoretical approaches have been compared with the experimental data from [21]. However, only in [19], calculations of the cluster geometries and polarizabilities have been performed on the same level of theory (i.e. all electron *ab initio*) as in our work and were limited by  $N \leq 8$ .

Alternatively, the jellium model for metal clusters was suggested. This model explains well enough the shell structure of metal clusters and their essential dynamic

properties, such as plasmon excitations. Initially, jellium calculations for metal clusters were based on the density functional formalism with the use of pseudopotentials for the description of electron relaxation effects and lattice structure [34]. Fully self-consistent calculations for spherical jellium metal clusters have been performed within the framework of the spin-density-functional method [35] and the Kohn-Sham formalism for the self-consistent determination of electron wave functions [36, 37]. The Hartree-Fock scheme for the self-consistent determination of the electron wave functions of spherical jellium metal clusters was also introduced later in [38, 39]. This approach was generalized for axially deformed cluster systems in [40]. Dynamical jellium model for metal clusters, which treats simultaneously collective vibrational modes (volume vibrations, i.e. breathing, plus shape vibrations) of the ionic jellium background in a cluster, the quantized electron motion and interaction between the electronic and ionic subsystems was developed in [41, 42].

The jellium model provides a very useful basis for studying various collision processes, such as photabsorption [43], photoionization [5, 44, 45], elastic [46, 47] and inelastic scattering [47–50], electron attachment [51, 52], photon emission [53, 54] and others, involving metal clusters,. On the basis of the jellium model one can develop *ab initio* many-body theories, such as the random phase approximation with exchange or the Dyson equation method and effectively solve many-electron correlation problem even for relatively large cluster systems containing up to 100 atoms or even more. Review of these methods in their application to the electron scattering of metal clusters one can find in [55]. As elucidated in the papers cited above, many-electron correlations are quite essential for the correct description of various characteristics of the cluster systems.

In spite of the fact that the jellium model with all its modifications is rather successful in explaining numerous phenomena involving metal clusters it obviously has its limits, because this model does not take into account the detailed ionic structure of clusters. The correspondence between predictions of the jellium model and the results of more advanced quantum chemistry calculations have not been performed in a systematic way so far. Partially, this is connected with the fact that quantum chemistry calculations are usually limited by small sizes of clusters, while the jellium model becomes adequate for larger cluster systems. Knowledge of the ranges of applicability of the jellium model and the level of its accuracy is important, because the jellium model often gives much more efficient theoretical basis particularly, when dealing with larger cluster systems.

In this paper we have undertaken detailed systematic theoretical study of structure and properties of sodium clusters beyond the jellium model using all-electron *ab initio* theoretical methods based on the Hartree-Fock approximation, density functional theory and perturbation theory, for clusters that size is large enough for jellium calculations. Namely, we have calculated optimized geometries of neutral and singly-charged sodium clusters consisting of up to 20 atoms, their multipole moments (dipole and quadrupole), static polarizabilities, binding energies per atom, ionization potentials and frequencies of normal vibration modes. We compare results of our calculations with

the available experimental data, results of other theoretical works performed both within the framework of the jellium model and beyond, using quantum chemistry methods, and elucidate the level of accuracy of different theoretical approaches. Also, we demonstrate the great role of many-electron correlations in the formation of structure and properties of small metal clusters. Our results form a good basis for the detailed study of dynamic properties of small metal clusters as well as structure and properties of other atomic cluster systems.

Our calculations elucidate the level of accuracy of various theoretical schemes for the treatment of electronic structure in metal clusters, which is important to know and is not obvious in advance due to complexity of theoretical methods involved. Some characteristics (dipole and quadrupole moments or spectra of normal vibration modes, for example), which we have calculated in this paper are new and were not studied before, at least according to our knowledge. These characteristics, however, might be, important, for instance, when considering dynamics of a cluster beam in an external non-homogeneous electric or magnetic field. Indeed, namely, cluster multipole moments should be responsible for the cluster isomers separation in the non-homogeneous external fields. We analyse the connection between the principal values of the cluster quadrupole moments tensor and the cluster shape (oblate, prolate or triaxially deformed).

The frequencies of the surface and volume vibration modes have been determined in the spectra of the cluster normal vibration frequencies and their correspondence to the predictions of the dynamical jellium model [41, 42] was established.

Our calculations have been performed with the use of the Gaussian 98 software package [56]. We have used the atomic system of units in this paper,  $\hbar = m_e = |e| = 1$  unless other units are not indicated.

## 2. Theoretical methods

In this work we are studying structure and properties of small sodium clusters on the basis of all-electron *ab initio* many-body theory methods. We calculate the optimized geometries of clusters consisting of up to  $N \leq 20$  atoms, where  $N$  is the number of atoms in the cluster. For the sequence of clusters with  $N \leq 20$ , we determine size dependence of the cluster ionization potentials, total energies, multipole moments (dipole and quadrupole), bonding distances and dipole polarizabilities. We also calculated and analyze vibration spectra of the clusters.

We have done these calculations using different theoretical schemes. We have calculated cluster characteristics in the all-electron Hartree-Fock approximation. This approximation does not take into account many-electron correlations in the system, which turn out to play essential role in the formation of clusters properties. Therefore, we also calculate all the characteristics using post Hartree-Fock theories accounting for many-electron correlations. Namely, this was done in the Møller and Plesset perturbation theory of the second and the fourth order and the three parameter Becke's gradient-corrected exchange functional with the gradient-corrected correlation

functional of Lee, Yang and Parr.

Below, we discuss theoretical methods used in our work. The aim of this discussion is to present essential ideas of the methods and give the necessary references, rather than to describe them in detail.

### 2.1. Hartree-Fock method (HF)

In the Hartree-Fock approximation, the many-electron wave function of a cluster is expressed as antisymmetrized product of the single-electron wave functions,  $\psi_i$ , of cluster electrons, which are also often called molecular orbitals. The Hartree-Fock equation for the determination of the molecular orbitals  $\psi_i$  reads as (see e.g. [57]):

$$(-\Delta/2 + U_{ions} + U_{HF})\psi_i = \varepsilon_i\psi_i. \quad (1)$$

Here, the first term represents the kinetic energy of the  $i$ -th electron, and  $U_{ions}$  describes its attraction to the ions in the cluster. The Hartree-Fock potential  $U_{HF}$  represents the Coulomb and the exchange interaction of the electron  $i$  with other electrons in the cluster,  $\varepsilon_i$  is the single electron energy.

In *Gaussian 98*, the molecular orbitals,  $\psi_i$ , are approximated by a linear combination of a pre-defined set of single-electron functions,  $\chi_\mu$ , known as basis functions. This expansion reads as follows:

$$\psi_i = \sum_{\mu=1}^N c_{\mu i} \chi_\mu, \quad (2)$$

where coefficients  $c_{\mu i}$  are the molecular orbital expansion coefficients,  $N$  is the number of basis functions, which are chosen to be normalized.

The basis functions  $\chi_\mu$  are defined as linear combinations of primitive gaussians:

$$\chi_\mu = \sum_p d_{\mu p} g_p, \quad (3)$$

where  $d_{\mu p}$  are fixed constants within a given basis set, the primitive gaussians,  $g_p = g(\alpha, \mathbf{r})$ , are the gaussian-type atomic functions having the following form:

$$g(\alpha, \mathbf{r}) = cx^n y^m z^l e^{-\alpha r^2} \quad (4)$$

Here,  $c$  is the normalization constant. The choice of the integers  $n$ ,  $m$  and  $l$  defines the type of the primitive gaussian function: s, p, d or f (for details see [58]).

Substituting these expansions in the Hartree-Fock equations (1), one can rewrite them in the form, known also as the Roothaan and Hall equations:

$$\sum_{\nu=1}^N (H_{\mu\nu} - \varepsilon_i S_{\mu\nu}) c_{\nu i} = 0 \quad \mu = 1, 2, \dots, N \quad (5)$$

Being written in the matrix form, this equation reads as:

$$HC = SC\varepsilon, \quad (6)$$

where each element is a matrix. Here,  $\varepsilon$  is a diagonal matrix of orbital energies, each of its elements  $\varepsilon_i$  is the single-electron energy of the molecular orbital  $\psi_i$ ,  $H$  is the Hamiltonian matrix as it follows from (1),  $S$  is the overlap matrix, describing the overlap between orbitals. For more details regarding this formalism see [58].

Equations (6) are none linear and must be solved iteratively. The procedure which does so is called the *Self-Consistent Field* (SCF) method.

The above written equations consider the restricted Hartree-Fock method. For the open shell systems, the unrestricted Hartree-Fock method has to be used. In this case, the alpha and beta electrons with spins up and down are assigned to different orbitals, resulting in two sets of molecular orbital expansion coefficients:

$$\begin{aligned}\psi_i^\alpha &= \sum_{\mu=1}^N c_{\mu i}^\alpha \chi_\mu \\ \psi_i^\beta &= \sum_{\mu=1}^N c_{\mu i}^\beta \chi_\mu,\end{aligned}\tag{7}$$

The two sets of coefficients result in two sets of the Hamiltonian matrices and the two sets of orbitals.

## 2.2. Møller-Plesset perturbation theory method ( $MP_n$ )

The Hartree-Fock theory provides an inadequate treatment of electrons motion within a molecular system, because it does not properly treat many-electron correlations. The many electron correlations can be accounted for using different methods. The most straightforward way for achieving this goal is based on the perturbation theory. Indeed, the total Hamiltonian,  $H$ , of the cluster can be divided into two parts

$$H = H_0 + V\tag{8}$$

Here  $H_0$  is the Hamiltonian corresponding to the Hartree-Fock level of theory and  $V$  is the residual interelectron interaction, which can be treated as a small perturbation.

Considering  $V$  as a small perturbation one can construct the solution of the Schrödinger equation for many-electron system in an arbitrary order of the perturbation theory. The perturbation theory of this type is well known since the work by Møller-Plesset [59] and can be found in numerous textbooks on quantum mechanics (see e.g. [60]).

Below we refer to this theoretical method as to the Møller-Plesset perturbation theory [59] of the second or forth order,  $MP_2$  or  $MP_4$ . Indices here indicate the order of the perturbation theory.

### 2.3. Density functional methods (B3LYP)

The density functional theory (DFT) is based upon a strategy of modelling electron correlation via general functionals of the electron density. Within the DFT one has to solve the Kohn-Sham equations, which read as (see e.g. [8,9,11–14])

$$\left(\frac{\hat{p}^2}{2} + U_{ions} + V_H + V_{xc}\right)\psi_i = \varepsilon_i\psi_i, \quad (9)$$

where the first term represents the kinetic energy of the  $i$ -th electron, and  $U_{ions}$  describes its attraction to the ions in the cluster,  $V_H$  is the Hartree part of the interelectronic interaction:

$$V_H(\vec{r}) = \int \frac{\rho(\vec{r}')}{|\vec{r} - \vec{r}'|} d\vec{r}', \quad (10)$$

and  $\rho(\vec{r}')$  is the electron density:

$$\rho(\vec{r}) = \sum_{\nu=1}^N |\psi_\nu(\vec{r})|^2, \quad (11)$$

where  $V_{xc}$  is the local exchange-correlation potential,  $\psi_i$  are the electronic orbitals and  $N$  is the number of electrons in the cluster.

The exchange-correlation potential is defined as the functional derivative of the exchange-correlation energy functional:

$$V_{xc} = \frac{\delta E_{xc}[\rho]}{\delta \rho(\vec{r})}, \quad (12)$$

The approximate functionals employed by DFT methods partition the exchange-correlation energy into two parts, referred to as *exchange* and *correlation* parts:

$$E_{xc}[\rho] = E_x(\rho) + E_c(\rho) \quad (13)$$

Physically, these two terms correspond to same-spin and mixed-spin interactions, respectively. Both parts are the functionals of the electron density, which can be of two distinct types: either *local* functional depending on only the electron density  $\rho$  or *gradient-corrected* functionals depending on both  $\rho$  and its gradient,  $\nabla\rho$ .

In literature, there is a variety of exchange correlation functionals. Below, we refer only to those, which are related to the calculation performed in this work.

The local exchange functional is virtually always defined as follows:

$$E_x^{LDA} = -\frac{3}{2}\left(\frac{3}{4\pi}\right)^{1/3} \int \rho^{4/3} d^3\mathbf{r} \quad (14)$$

This form was developed to reproduce the exchange energy of a uniform electron gas. By itself, however, it is not sufficient for the adequate description of atomic clusters.

The gradient-corrected exchange functional introduced by Becke [61] and based on the LDA exchange functional reads as:

$$E_x^{B88} = E_x^{LDA} - \gamma \int \frac{\rho^{4/3} x^2}{1 + 6\gamma \sinh^{-1} x} d^3\mathbf{r} \quad (15)$$

where  $x = \rho^{-4/3} |\nabla \rho|$  and  $\gamma = 0.0042$  is a parameter chosen to fit the known exchange energies of the noble gas atoms.

Analogously to the above written exchange functionals, there are local and gradient-corrected correlation functionals, for example, those introduced by Perdew and Wang [62] or by Lee, Yang and Parr [63]. Their explicit expressions are somewhat lengthy and thus we do not present them here and refer to the original papers.

In the pure DFT, an exchange functional usually pairs with a correlation functional. For example, the well-known BLYP functional pairs Becke's gradient-corrected exchange functional (15) with the gradient-corrected correlation functional of Lee, Yang and Parr [63].

In spite of the success of the pure DFT theory in many cases, one has to admit that the Hartree-Fock theory accounts for the electron exchange the most naturally and precisely. Thus, Becke has suggested [61] functionals which include a mixture of Hartree-Fock and DFT exchange along with DFT correlations, conceptually defining  $E_{xc}$  as:

$$E_{xc}^{mix} = c_{HF} E_x^{HF} + c_{DFT} E_{xc}^{DFT}, \quad (16)$$

where  $c_{HF}$  and  $c_{DFT}$  are constants. Following this idea, a Becke-type three parameter functional can be defined as follows:

$$\begin{aligned} E_{xc}^{B3LYP} = & E_x^{LDA} + c_0(E_x^{HF} - E_x^{LDA}) + c_x(E_x^{B88} - E_x^{LDA}) + \\ & + E_c^{VWN3} + c_c(E_c^{LYP} - E_c^{VWN3}) \end{aligned} \quad (17)$$

Here,  $c_0 = 0.2$ ,  $c_x = 0.72$  and  $c_c = 0.81$  are constants, which were defined by fitting to the atomization energies, ionization potentials, proton affinities and first-row atomic energies [58].  $E_x^{LDA}$  and  $E_x^{B88}$  are defined in (14) and (15) respectively.  $E_x^{HF}$  is the functional corresponding to Hartree-Fock equations (1). The explicit form for the correlation functional  $E_c^{VWN3}$  as well as for gradient-corrected correlation functional of Lee, Yang and Parr,  $E_c^{LYP}$ , one can find in [64] and [63] correspondingly. Note that instead of  $E_c^{VWN3}$  and  $E_c^{LYP}$  in (17) one can also use the Perdew and Wang correlation functional [62].

#### 2.4. Geometry optimization

The cluster geometries, which we have calculated in our work, have been determined using the geometry optimization procedure. This procedure implies the calculation of the multidimensional potential energy surface for a cluster and then finding local minima on this surface. The key point for this search is fixing the starting geometry of the cluster, which could converge during the calculation to the local or global minimum. There is no unique way in achieving this goal with *Gaussian 98*.

In our calculations, we have created the starting geometries empirically, often assuming certain cluster symmetries. Note, that during the optimization process the

geometry of the cluster as well as its initial symmetry sometimes change dramatically. All the characteristics of clusters, which we have calculated and presented in next section, are obtained for the clusters with optimized geometry.

In our calculations, we have made no assumptions on the core electrons in the optimized clusters, which means that all electrons available in the system, have been taken into account, when computing potential energy surface. For clusters with  $N > 10$ , this process becomes rather computer time demanding. Thus, in this work we have limited our calculations by clusters consisting up to  $N \leq 20$ .

### 2.5. Normal vibrations

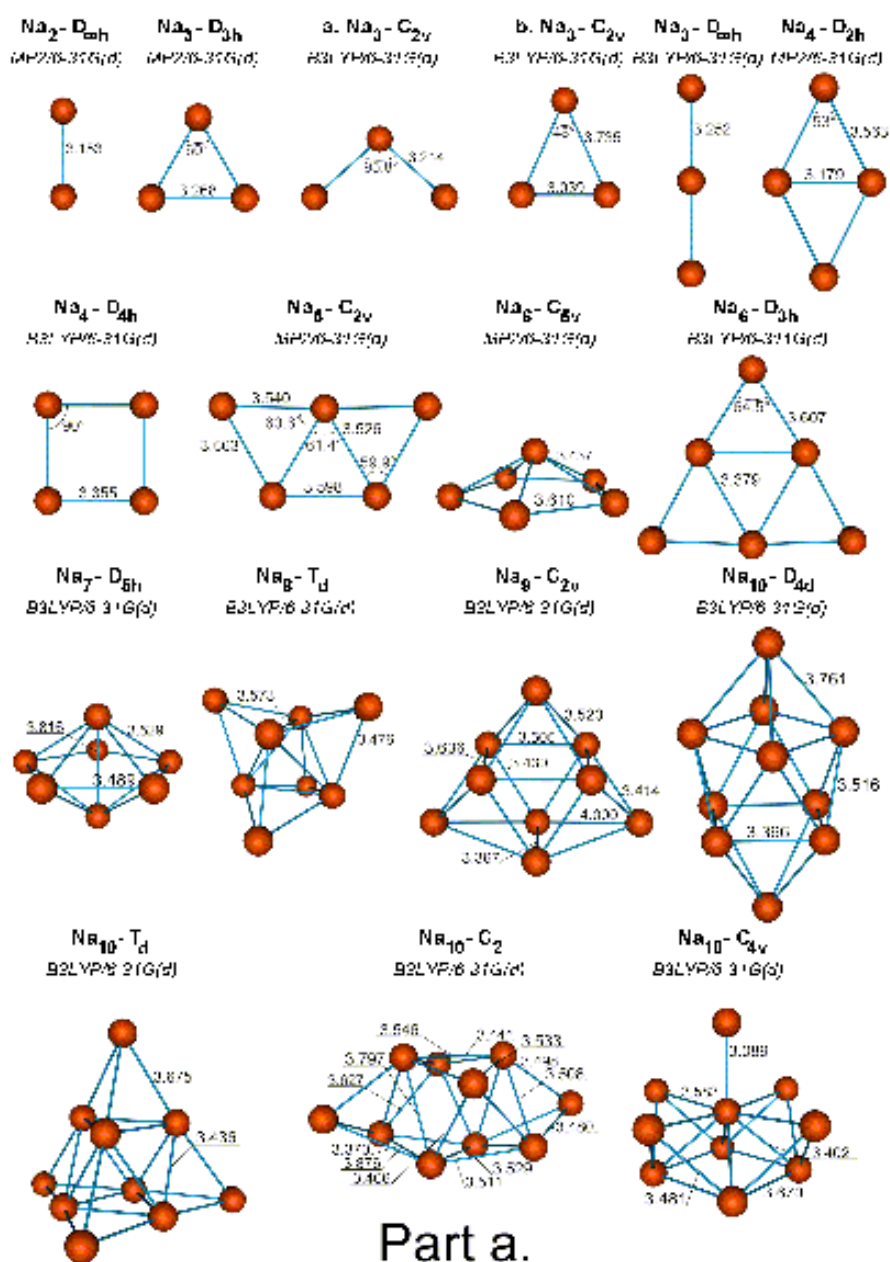
Knowledge of the potential energy surface in the vicinity of a local minimum, allows one easily to determine corresponding normal vibration modes of the system. We have performed such calculation and determined the vibration energy spectrum for a number of clusters. Particular attention in this calculation has been paid to the identification of the breathing and the surface vibration modes and comparison their frequencies with those predicted in [41, 42] for spherical sodium clusters on the basis of the dynamical jellium model.

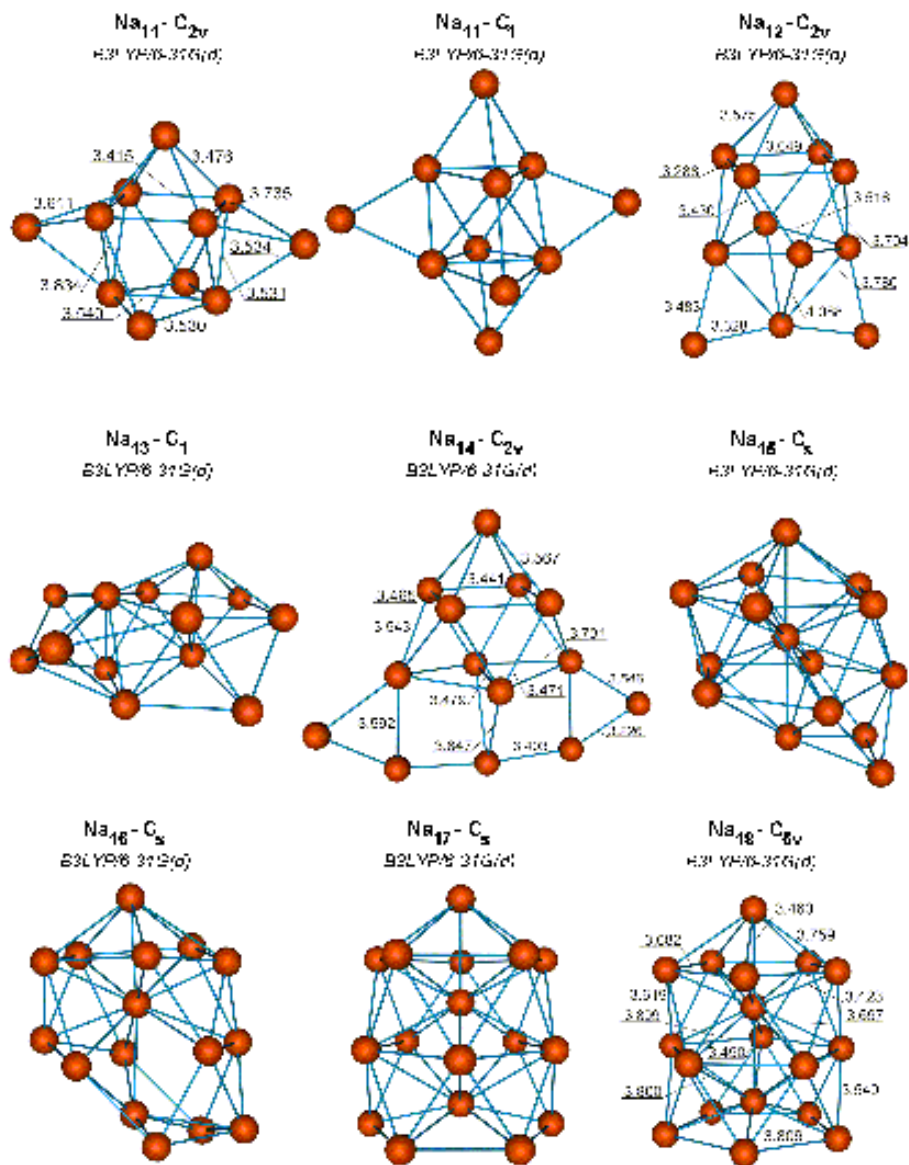
## 3. Results of calculations and discussion

In this section we present the results of calculations performed with the use of methods described above. We have calculated the optimized geometries of neutral and singly charged sodium clusters consisting of up to 20 atoms, their multipole moments (dipole and quadrupole), static polarizabilities, binding energies per atom, ionization potentials and frequencies of the normal vibration modes. We compare results of our calculations with the available experimental data and the results of other theoretical works performed both within the framework of the jellium model and beyond, using quantum chemistry methods and establish the level of accuracy of different theoretical approaches. Particular attention is paid to the clusters in the range  $10 < N < 20$ , because some characteristics of the clusters in this size range have been calculated on the *ab initio* basis in our paper for the first time. Also, we demonstrate the great role of many-electron correlations in the formation of structure and properties of small metal clusters.

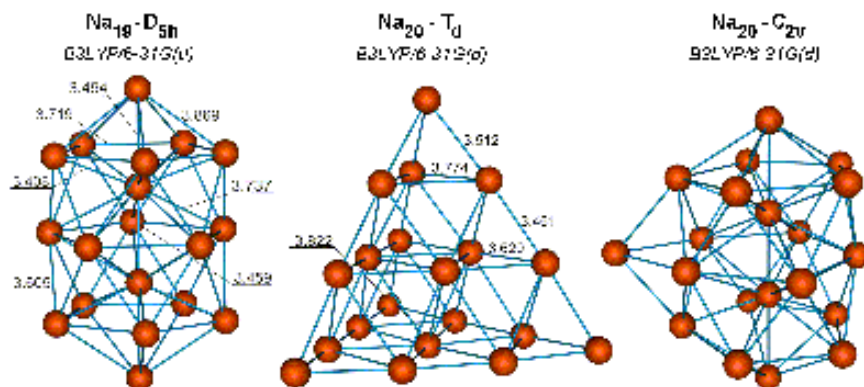
### 3.1. Geometry optimization of $Na_n$ and $Na_n^+$ clusters

Results of the cluster geometry optimization for neutral and singly charged sodium clusters consisting of up to 20 atoms shown in figures 1 and 2 respectively. The cluster geometries have been determined using the methodology described in section 2. Namely, the optimization of the cluster geometries has been performed with the use of *B3LYP* and *MP<sub>2</sub>* methods.



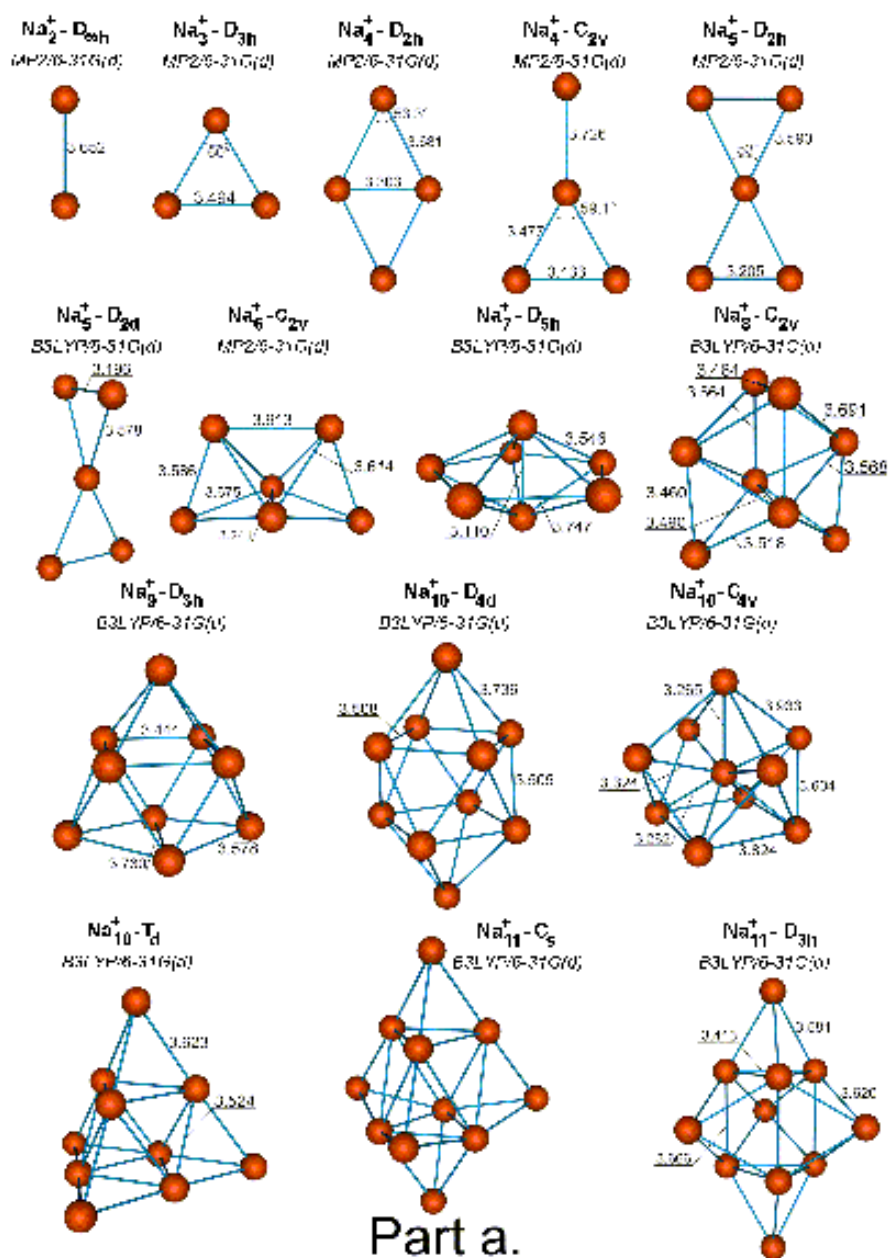


Part b.



## Part c.

**Figure 1.** Optimized geometries of neutral sodium clusters  $Na_2 - Na_{10}$  (part a),  $Na_{11} - Na_{18}$  (part b) and  $Na_{19} - Na_{20}$  (part c). The interatomic distances are given in angstroms. The label above each cluster image indicates its point symmetry group and the calculation method by which the cluster was optimized.



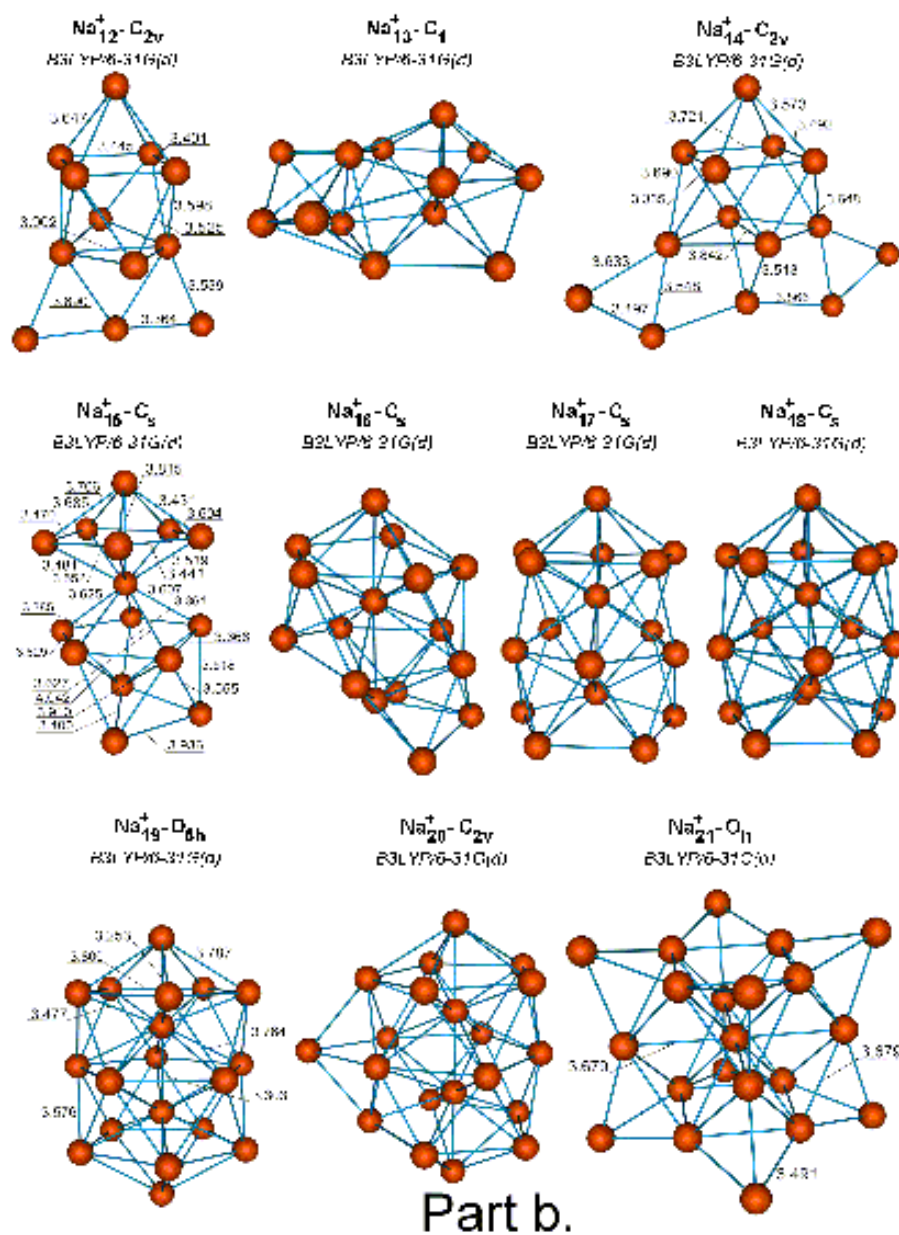


**Figure 2.** Optimized geometries of singly charged sodium clusters  $Na_{12}^+ - Na_{11}^+$  (part a) and  $Na_{12}^+ - Na_{21}^+$  (part b). The interatomic distances are given in angstroms. The label above each cluster image indicates the point symmetry group and the calculation method by which the cluster was optimized.

For clusters with  $N \leq 6$ , we preferably used the  $MP_2$  method. This method leads to the results, which are in a reasonable agreement with those derived by other methods (see e.g. [16, 17]). For example, the side bond length in the rhomboidal  $Na_4$  cluster calculated in [16] by the all-electron Hartree-Fock method is equal to 3.74 Å, while in our case it is equal to 3.56 Å. The smaller diagonal value for  $Na_4$  is equal to 3.25 Å in [16], while we determine it as 3.18 Å.

The  $MP_2$  method becomes more and more computer time demanding with the growth cluster size. This happens due to increase in a number of integrals involved in the computations. It turns out that for larger cluster systems the  $B3LYP$  method is more efficient. The accuracy of the  $B3LYP$  method is comparable with the accuracy of the  $MP_2$  method, as it is clear from the comparison of the  $B3LYP$  and  $MP_2$  cluster geometries with those computed in [16] by the configuration interaction method.

Clusters of a certain size can possess various isomer forms, those number grows dramatically with increasing cluster size. We illustrate the situation, and calculate several isomers of the the  $Na_3$ ,  $Na_6$ ,  $Na_{10}$ ,  $Na_{11}$  and  $Na_{20}$  clusters. They all are presented in figure 1. Note, that the linear and equilateral triangular  $Na_3$  isomers, have not been described in the earlier papers [15–17] (see also [11, 13, 14]), in which isosceles triangular isomers were considered. The comparison of properties (dipole and quadrupole moments, total energies, bonding distances) of these clusters will be given below.

On the example of the  $Na_4$  cluster, we demonstrate how the multiplicity of an electronic state of the system can influence its geometry. Figure 1 shows that the  $Na_4$  cluster has the rhomboidal geometry corresponding to the  $D_{2h}$  point symmetry group, if the multiplicity of the cluster is equal to 1, while, for the multiplicity being equal to 3, the cluster has the quadratic geometry characterised by the  $D_{4h}$  point symmetry group.

Sodium clusters with  $N \leq 5$  have the plane structure, while for  $N = 6$  both plane and spatial isomers are possible. This feature is consistent with the jellium picture and can be explained from the minimization principle for the cluster surface. Indeed, the surface of small plane cluster isomers is less in comparison with the surface of their possible spatial forms.

Comparison of geometries of the neutral and singly-charged clusters presented in figures 1 and 2 shows their significant difference. For smaller sizes ( $N \leq 8$ ), singly-charged and neutral clusters have sometimes different point symmetry groups and bonding distances (see images of the  $Na_4$ ,  $Na_5$ ,  $Na_6$  and  $Na_8$  clusters and their ions). The alteration in the geometry of cluster ions occurs due to the excessive positive charge available in the system. The structural change of cluster ions becomes less profound with increasing cluster size, see clusters with  $N \geq 10$ , because the excessive positive charge in this case turns out to be insufficient to produce substantial change in a massive cluster, although sometimes (compare  $Na_{15}$  and  $Na_{15}^+$ ) noticeable change in the cluster geometry is also possible.

The striking difference in geometries of small singly charged and neutral clusters is closely linked to the problem of cluster fission. It is natural to assume that with

increasing cluster charge small clusters should become unstable and fragment into two parts, while for larger cluster sizes one can expect quasi-stable configurations, which should decay via the fission process. Calculation of such configurations is an interesting task, because it may provide the essential information on the predominant fission channels in the system. We do not perform such an analysis in our work, but draw attention that geometries of the cluster ions, like  $Na_4^+$ ,  $Na_5^+$ ,  $Na_6^+$  and  $Na_{15}^+$ , lead to the obvious hints on the possible fragmentation channels in these cluster systems.

Figure 1 shows that the clusters  $Na_8$  and  $Na_{20}$  have the higher point symmetry group  $T_d$  as compared to the other clusters. This result is in a qualitative agreement with the jellium model. According to the jellium model [36–40], clusters with closed shells of delocalized electrons have the spherical shape, while clusters with opened electron shells are deformed. The jellium model predicts spherical shapes for the clusters with the magic numbers  $N = 8, 20, 34, 40, \dots$ , having respectively the following electronic shells filled:  $1s^2 1p^6, 1d^{10} 2s^2, 1f^{14}, 2p^6, \dots$ .

We have also found the  $T_d$  symmetry group isomer for the  $Na_{10}$  cluster. However, this cluster isomer is not the lowest energy isomer of  $Na_{10}$  (see table A1). The similar situation occurs in the jellium model, where the  $1s^2 1p^6, 2s^2$  closed shell electronic configuration does not minimize the cluster total energy.

Note also, that both the *LDA* and *HF* jellium models predict some deviation from sphericity for the  $Na_{18}$  cluster [40] having  $1d$  subshell filled, which is a result of electron configurations mixing. This fact is also in a qualitative agreement with the results of our *ab initio* calculations. The point group symmetry of the  $Na_{18}$  cluster,  $C_{5v}$ , is lower than  $T_d$ , which is the point symmetry group for the  $Na_8$  and  $Na_{20}$  clusters, and even lower than the point symmetry group for some opened shell clusters, like  $Na_7$  and  $Na_{19}$ , having the point symmetry group  $D_{5h}$ .

Note that there are some clusters possessing relatively low point symmetry group, that nevertheless is quite close to the higher point symmetry group. The higher symmetry breaking is not occasional and can be explained via the Jahn-Teller effect [60]. Such situation occurs, for example, in the  $Na_9$  and  $Na_{11}$  clusters, which possess the  $C_{2v}$  point symmetry group, but their geometry is close to the geometry of the  $D_{3h}$  group.

The jellium prediction on the sphericity of the magic clusters works not so well for cluster ions. Indeed, the geometry and the point symmetry group of  $Na_9^+$  does not allow one to state the higher sphericity of this cluster as compared to its neighbours. The analysis of the quadrupole moments and cluster deformations performed below demonstrates this conclusion quite clearly. This happens because forces emerging in the cluster during its transition from neutral to singly charged state turns out to be insufficient to rearrange the cluster geometry from deformed to spherical one.

We have found two isomers of the  $Na_{20}$  cluster, which have rather regular structure and differ significantly one from another. The cluster geometries presented in figure 1 allow one to assume that there exist at least two independent paths of the cluster

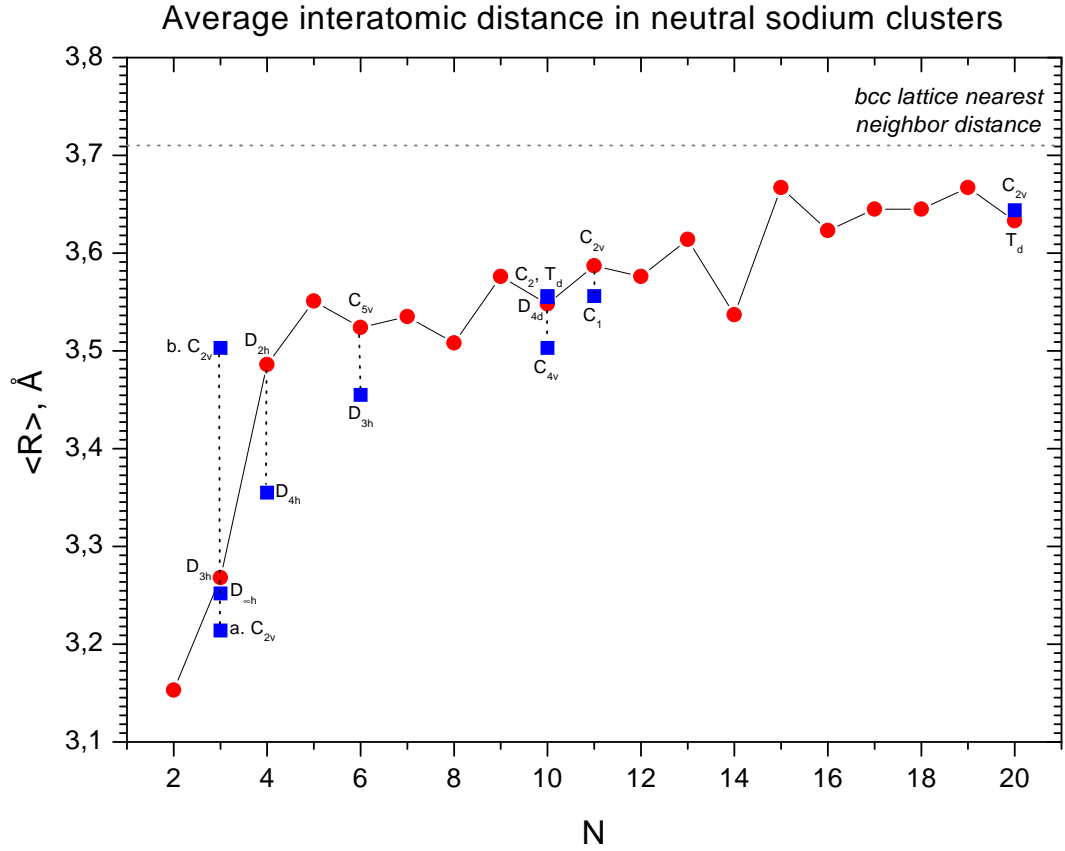
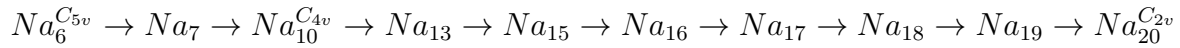
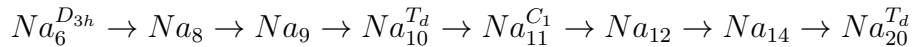


**Figure 3.** Averaged bonding distance as a function of cluster size for optimized geometries of neutral sodium clusters. For some cluster numbers more than one isomer has been considered. In these cases, labels indicate the point symmetry group of the corresponding isomers. Geometries of the optimized clusters one can find in figure 1.

structure formation. Indeed, the following isomers



probably belong to the chain leading to the formation of the  $C_{2v}$  isomer of the  $Na_{20}$  cluster, while the clusters



form the path on which the  $T_d$  isomer of the  $Na_{20}$  cluster is formed. Figure 1 clearly shows the steps of the cluster formation process along these two paths. Although, for most of  $N$ , we have calculated isomers belonging to one path or another, it is natural to assume that the two different type of geometries exist for all  $N$ , similar to how it happens for  $Na_6$  and  $Na_{20}$  clusters. For clusters smaller than  $Na_6$ , one can not distinguish the two paths clearly enough as it is seen from figure 1. Conclusions made

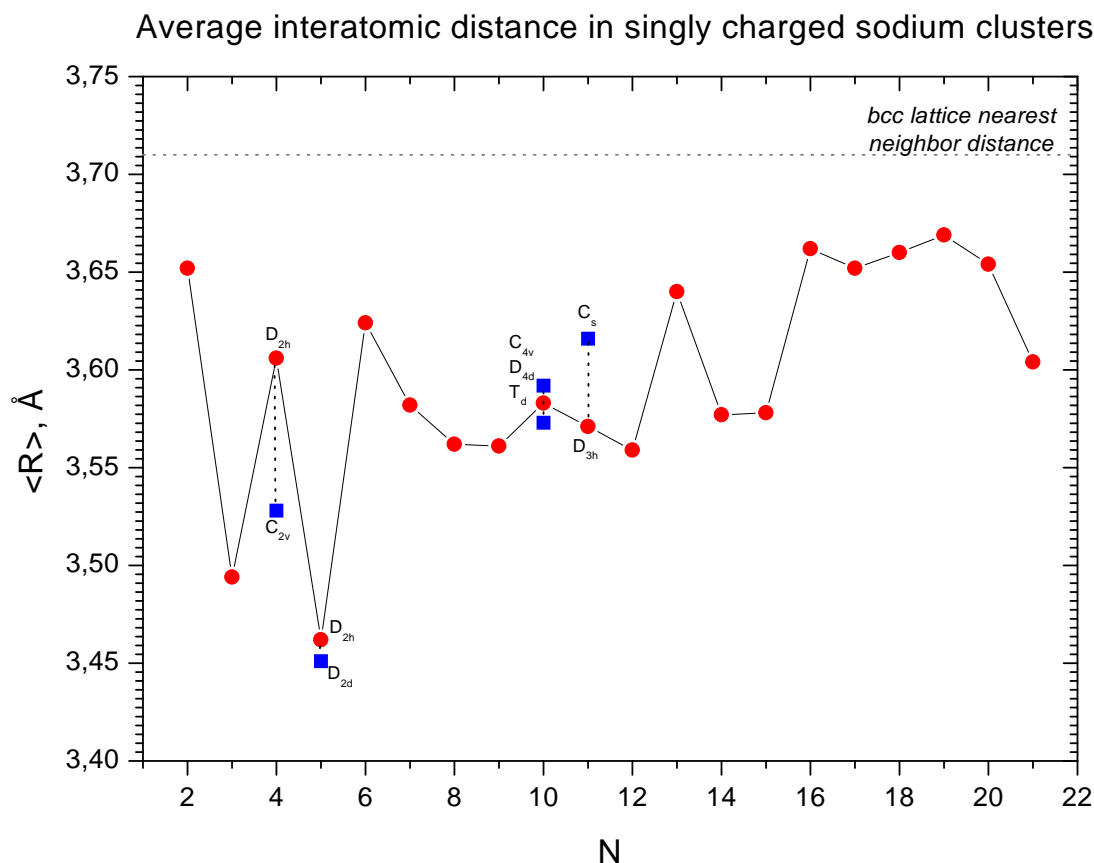


**Figure 4.** Averaged bonding distance as a function of cluster size for optimized geometries of singly charged sodium clusters. For some cluster numbers more than one isomer has been considered. In these cases, labels indicate the point symmetry group of the corresponding isomers. Geometries of the optimized clusters one can find in figure 2.

for neutral clusters regarding the growing process are applicable to the great extent to singly charged cluster ions as it is clear from figure 2, although cluster ions geometries sometimes differ substantially from their neutral prototypes.

Cluster geometries allow one easily to compute and analyze the average bonding distance as a function of cluster size. The result of this analysis for neutral and singly charged sodium clusters is presented in figures 3 and 4. These figures show how the average bonding distance converge to the bulk limit indicated in the figures by horizontal lines. When calculating the average bonding distance in a cluster, interatomic distances smaller than  $4.1 \text{ \AA}$  have only been considered. This upper limit on the interatomic distances has been chosen as a distance, which is 10 per cent larger than to the bcc-lattice nearest neighbour distance in the bulk sodium.

Figures 3 and 4 show that the dependence of the average bonding distance,  $\langle R \rangle$ , on

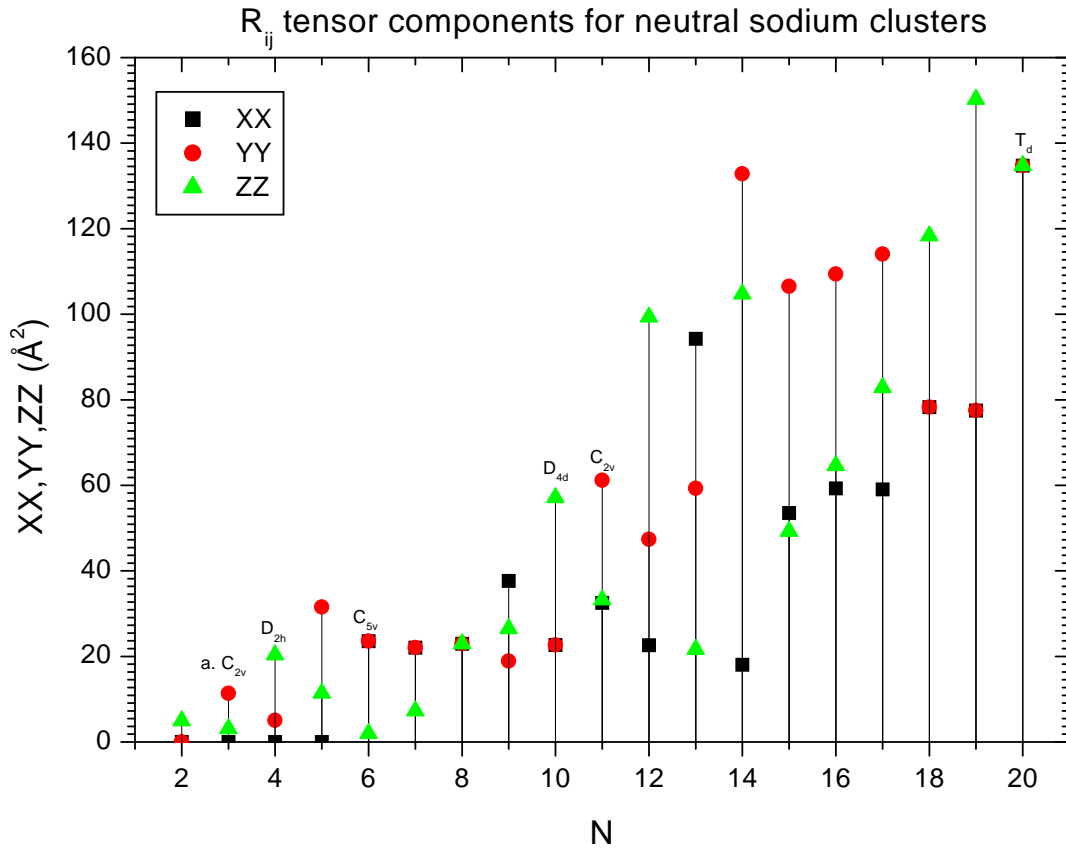


**Figure 5.** The principal values of tensor  $R_{ij}$  for optimized neutral sodium clusters as a function of cluster size calculated by the  $B3LYP$  method. Squares, circles and triangles represent the  $R_{xx}$ ,  $R_{yy}$  and  $R_{zz}$  tensor principal values respectively. For some clusters, more than one isomer has been considered. In these cases, labels indicate the point symmetry group of the corresponding isomers. Geometries of the optimized clusters one can find in figure 1.

cluster size is non-monotonous. For neutral clusters, one can see odd-even oscillations of  $\langle R \rangle$  atop its systematic growth and approaching the bulk limit. These features have the quantum origin and can be explained by the delocalization of valence atomic electrons. Indeed, the odd-even oscillations arise due to the spin pairing of the delocalised electrons. This type of behaviour is also typical for other cluster characteristics and will be discussed below in more detail. Relatively large increase of the average distance, seen for small sodium cluster ions with  $N \leq 9$ , is also qualitatively clear. It can be explained by the Coulomb instability developing in the cluster with increasing its ionization rate.

Cluster shape can be characterized by the oblate, prolate or triaxial deformation. The prolate deformation of the cluster is characterized by larger distortion of the ionic charge distribution along z-axis as compared to distortions along x- and y axes. In the oblate deformation case the situation is opposite. Deformations of the ionic charge



the relations:  $R_x = \sqrt{R_{xx}/N}$ ,  $R_y = \sqrt{R_{yy}/N}$  and  $R_z = \sqrt{R_{zz}/N}$ . Note that tensor  $R_{ij}$  is closely connected with the cluster moment of inertia tensor and the quadrupole moment tensor of the ionic distribution.

In figures 5 and 6 we present the principle values  $R_{xx}$ ,  $R_{yy}$  and  $R_{zz}$  for a sequence of neutral and singly charged clusters respectively. Figures 5 and 6 demonstrate how the cluster deformation change as a function of cluster size. Figure 5 shows that all three principle values are equal for the tetrahedron group isomers of the magic clusters  $Na_8$  and  $Na_{20}$ . This feature is in the qualitative agreement with the jellium model, which predicts spherical shapes for the magic clusters. In many cases two of three principal values of  $R_{ij}$  are equal or nearly equal. Using the definition of the prolate and oblate cluster distortions given above and figures 5 and 6, one can easily determine the type of cluster deformation. For example, clusters  $Na_2$ ,  $Na_{10}$ ,  $Na_{18}$  and  $Na_{19}$  have the prolate deformation along z-principle axis, because the following condition  $R_{xx} = R_{yy} < R_{zz}$  is fulfilled. The clusters  $Na_6$  and  $Na_7$  possess the prolate deformation because in this case  $R_{xx} = R_{yy} > R_{zz}$ . Figures 5 and 6 show that most of clusters are triaxially deformed. However, it is often possible to assign clusters triaxially deformed prolate or oblate shape, because two of three principle values are close to each other. Thus, for instance,  $Na_4$ ,  $Na_{15}$  are triaxially prolate clusters, while  $Na_{14}$  is a triaxially oblate one. Figures 5 and 6 also show the relative value of prolate and oblate deformations in various clusters.

One can define a tensor analogous to  $R_{ij}$ , but for electrons. We do not plot the principle values of such a tensor because they are very close in absolute value to the principle values shown in figures 5 and 6 and could be traced from the principle values of the cluster total quadrupole moment tensor considered below in subsection 3.4.

### 3.2. Binding energy per atom for small neutral and singly-charged sodium clusters.

The binding energy per atom for small neutral and singly-charged sodium clusters is defined as follows:

$$E_b/N = E_1 - E_N/N \quad (18)$$

$$E_b^+/N = ((N-1)E_1 + E_1^+ - E_N^+)/N, \quad (19)$$

where  $E_N$  and  $E_N^+$  are the energies of a neutral and singly-charged N-atomic cluster respectively.  $E_1$  and  $E_1^+$  are the energies of a single sodium atom and an ion.

Figures 7 and 8 show the dependence of the binding energy per atom for neutral and singly-charged clusters as a function of cluster size. The energies of clusters have been computed using the *B3LYP*, *MP4* and *HF* methods described in section 2. For clusters with  $N \leq 8$ , computations of the energies have been performed by the three methods for the sake of comparison. We wanted to compare the methods by their accuracy and computation efficiency. The results of our calculations have also been compared with those derived by the configuration interaction (*CI*) method in [15–17]). Figures 7 and 8 demonstrate that the results of the *MP4* and *B3LYP* methods are in a reasonable

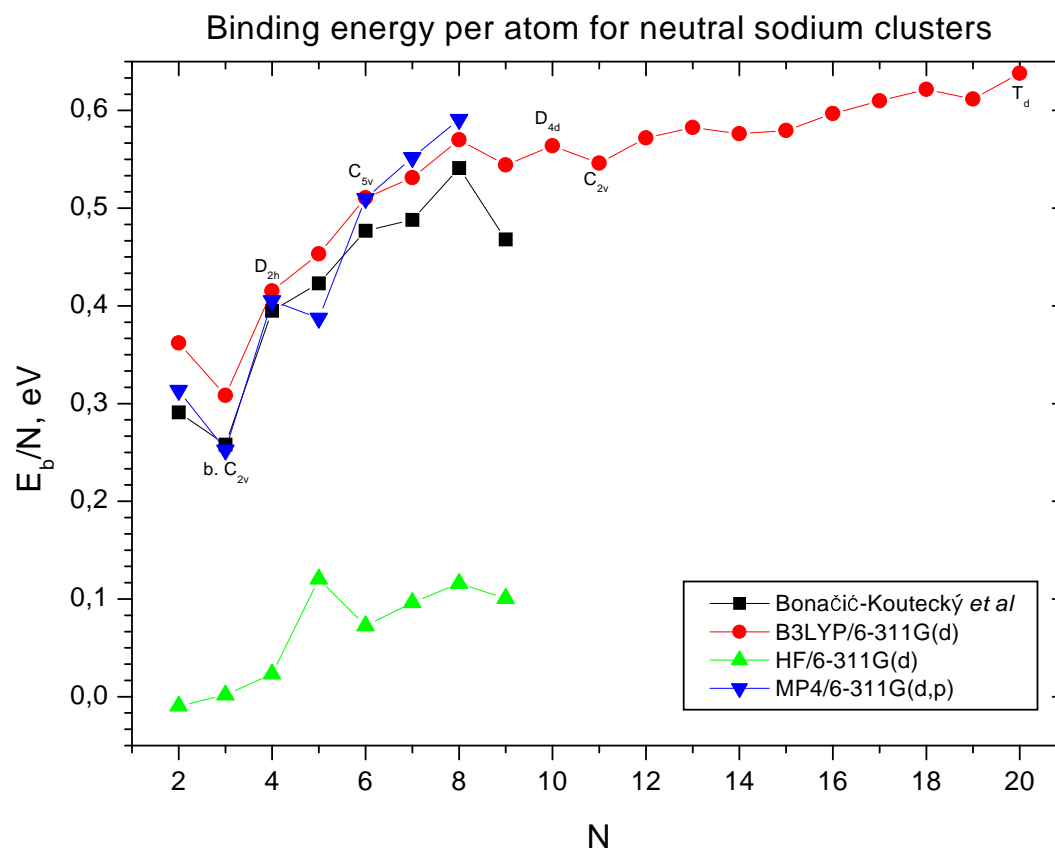


**Figure 7.** Binding energy per atom for neutral sodium clusters as a function of cluster size. Circles represent the binding energies per atom calculated by the *B3LYP* method, lower and upper triangles correspond to the energies obtained by the *MP*<sub>4</sub> method and in the *HF* approximation respectively. Squares show the result of the configuration interaction approach from the work by Bonačić-Koutecký *et al* (for details see [16,18]). Some points in figure have labels, indicating the point symmetry group of the isomers represented. Geometries of the corresponding clusters one can find in figure 1.

agreement with each other and with the *CI* results. The *HF* points significantly differ from the *MP*<sub>4</sub>, *B3LYP* and *CI* ones, which demonstrates the importance of many-electron correlations, taken into account in the *MP*<sub>4</sub>, *B3LYP* and *CI* methods and omitted in the *HF* approximation. Note that the energy of *Na*<sub>2</sub>, if computed in the pure *HF* approximation, is close to zero, which means that bonding in this molecule takes place mainly due to many-electron correlations.

The energies of clusters larger than *Na*<sub>8</sub> and *Na*<sub>8</sub><sup>+</sup> have been computed by the *B3LYP* method only, because this method is more efficient than *MP*<sub>4</sub> and the accuracy of both methods is comparable.

Figures 7 and 8 demonstrate the even-odd oscillation behaviour in the dependence

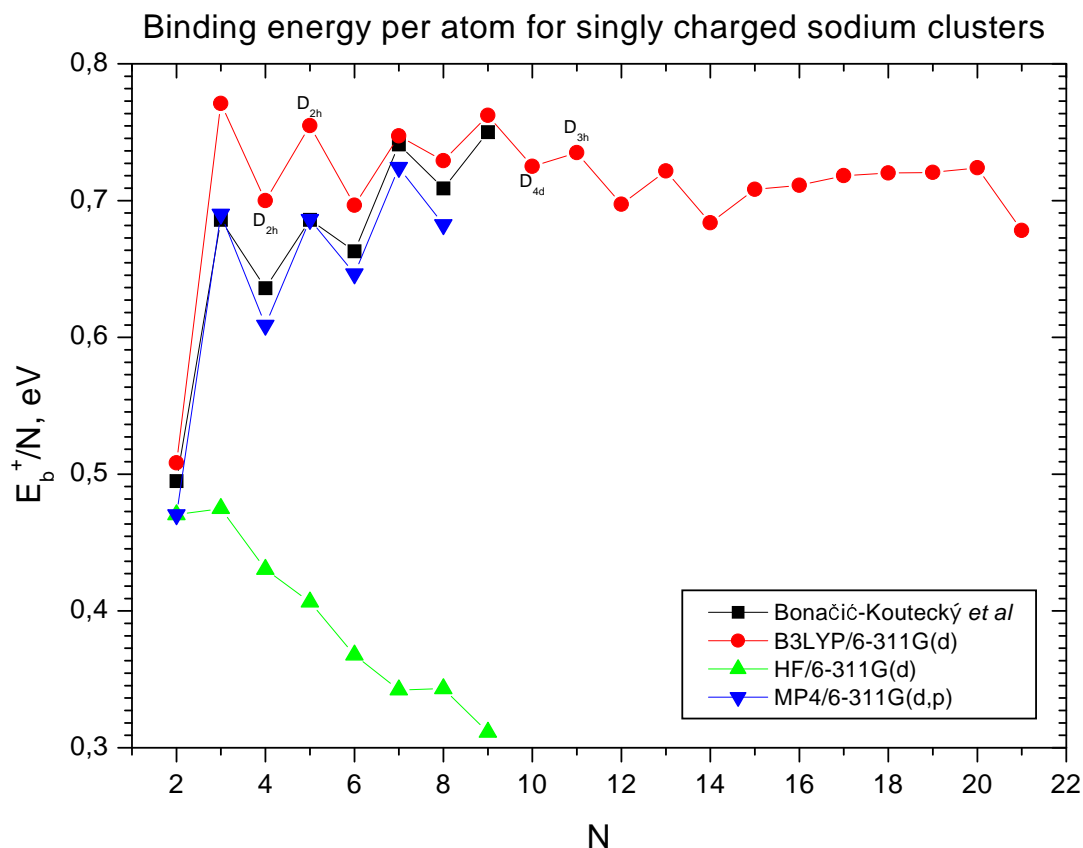


**Figure 8.** Binding energy per atom for singly charged sodium clusters as a function of cluster size. Circles represent the binding energies per atom calculated by the *B3LYP* method, lower and upper triangles correspond to the energies obtained by the *MP4* method and in the *HF* approximation respectively. Squares show the result of the configuration interaction approach from the work by Bonačić-Koutecký *et al* (for details see [16,18]). Some points in figure have labels, indicating the point symmetry group of the isomers represented. Geometries of the corresponding clusters one can find in figure 2.

of binding energy on cluster size. Indeed, for singly charged clusters, odd numbers corresponding to the singlet multiplicity have higher energies as compared to their even neighbours. Analogous situation takes place for neutral clusters. In this case, even cluster numbers have higher binding energies as compared to their odd neighbours. Note that for neutral clusters this phenomenon occurs simultaneously with slight systematic growth of the binding energies per atom with increasing cluster size.

Figures 7 and 8 also show that the binding energy per atom in the magic neutral clusters,  $Na_8$  and  $Na_{20}$ , is a little higher as compared to other clusters of the close size. The similar situation takes place for the  $Na_9^+$  cluster in the ionic case. This feature can be qualitatively understood on the basis of the jellium model: increasing the magic

clusters binding energy takes place due to the delocalised electrons shell closure. Note that the binding energy per atom for the magic  $Na_{21}^+$  turns out to be smaller than that for the neighbouring cluster ions. This happens because this particular cluster ion isomer is characterized by the  $O_h$  point symmetry group. Cluster isomers based on this point symmetry group usually have the lower binding energy per atom as compared to the isomers based on the icosahedron point symmetry group like those with  $N \geq 13$  shown in figures 1 and 2.

Tables A1 and A2 given in Appendix A provide the accurate values of the cluster total energies calculated by  $MP_4$ ,  $B3LYP$  and  $HF$  methods. For neutral clusters with  $N \leq 8$ , we also present the cluster energies calculated in [16] by the  $CI$  method. The values given in these tables have been used to plot figures 7 and 8. For some clusters, energies of different symmetry isomers are also given in the tables.

### 3.3. Ionization potentials

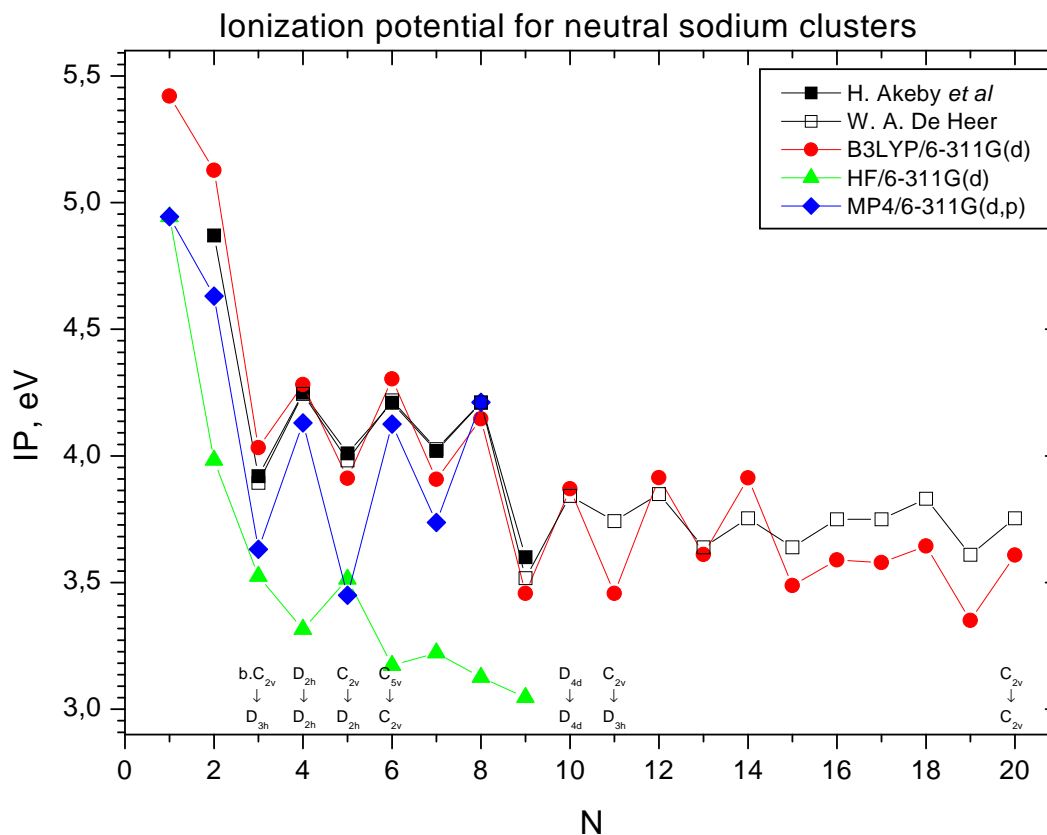
Let us now consider how the ionization potentials of sodium clusters evolve with increasing cluster size. Experimentally, such a dependence has been measured for sodium clusters in [8, 20].

The ionization potential of a cluster consisting of  $N$  atoms is defined as a difference between the energy of the singly-charged and neutral clusters:

$$IP = E_N^+ - E_N \quad (20)$$

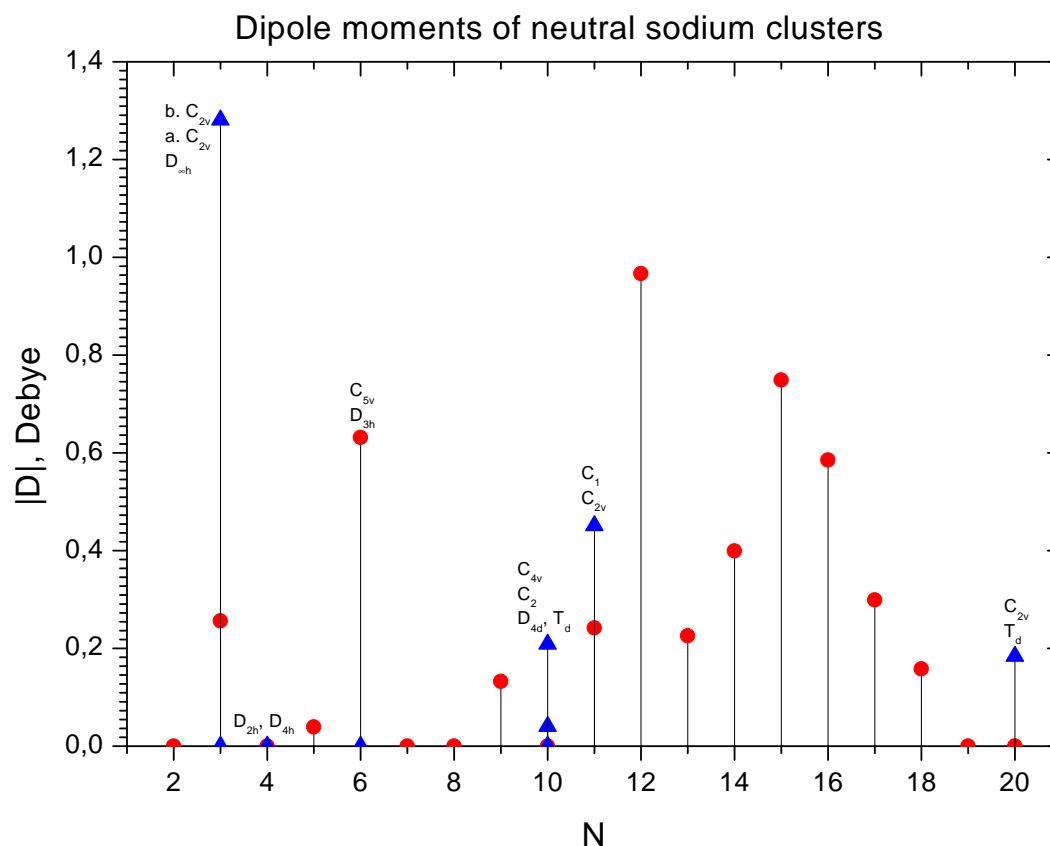
Figure 9 shows the dependence of the clusters ionization potential on  $N$ . Figure 9 demonstrates the comparison of the results derived by different methods,  $B3LYP$ ,  $MP_4$  and  $HF$  (see section 2), with the experimental data from [8] and [20]. The results of the  $B3LYP$  and  $MP_4$  methods are in a reasonable agreement with the experimental data, while the ionization potentials calculated on the basis of the  $HF$  approximation differ substantially from the experimental observations. This comparison shows the role of many-electron correlations in the formation of the cluster ionization potentials. The correlation effects are taken into account by the  $B3LYP$  and  $MP_4$  methods and omitted in the  $HF$  approximation.

Figure 9 demonstrates that the ionisation potentials drop with increasing cluster size, which is consistent with predictions of the classical spherical droplet model. However, this process has many irregularities, which have quantum origin. Indeed, the dependencies derived by the  $MP_4$  and  $B3LYP$  methods as well as the experimental one have a prominent odd-even oscillatory tendency. The maxima in these dependences correspond to the even- $N$ -clusters, which means their higher stability as compared to the neighbouring odd- $N$ -clusters. This happens because the multiplicities of the even- and odd- $N$ -clusters are different, being equal to one and two correspondingly. Interestingly enough that the  $B3LYP$  method reproduces correctly even the experimentally observed irregularity in the odd-even oscillatory behaviour, which happens at  $N = 16$  and  $N = 17$ , and some other minor details of the experimental data.



**Figure 9.** Ionization potentials of neutral sodium clusters as a function of cluster size. Circles show the results derived by the *B3LYP* method. Triangles and rhomboids represent the ionization potentials calculated by the *HF* and *MP<sub>4</sub>* methods respectively. Filled and open squares are the experimental values taken from [20] and [8] respectively. For some clusters, more than one neutral and/or singly charged cluster isomer has been considered. In these cases, labels indicate the point symmetry group of the initial neutral and the final charged cluster isomers used for the calculation of the ionization potential.

A significant step-like decrease in the ionization potential value happens at the transition from the dimer to the trimer cluster and also in the transition from  $Na_8$  to  $Na_9$ . Such an irregular behaviour can be explained by the closure of the electronic 1s- and 1p-shells of the delocalized electrons in the clusters  $Na_2$  and  $Na_8$  respectively. The next significant drop in the ionization potential value takes place in the transition from the magic  $Na_{20}$  to the  $Na_{21}$  cluster.



**Figure 10.** Dipole moments of the optimized neutral sodium clusters as a function of cluster size calculated by the *B3LYP* method. For some clusters, more than one isomer has been considered. In these cases, labels indicate the point symmetry group of corresponding isomers. Geometries of the optimized clusters one can find in figure 1. 1 Debye=0.3935 a.u.

### 3.4. Multipole moments

We have calculated multipole moments (dipole, quadrupole, octapole and hexadecapole) for the sodium clusters whose geometry is shown in figures 1 and 2. In figures 10 and 11, we plot the absolute values of the dipole moments for the neutral and singly charged sodium clusters as a function of cluster size.

The dipole moments of some sodium clusters (see figure 10), which we predict in our paper, arise due to the fact that the electron charge distribution not always matches the ionic charge distribution and can be shifted with respect to the cluster centre of mass. Our calculations show that only clusters with the C-point symmetry groups, like the isosceles triangle isomers of  $Na_3$ , the pentagonal  $Na_6$  pyramid isomer,  $Na_{12}$ ,  $Na_{18}$  and others, possess dipole moments. These clusters have either an axis of a certain order or a plane of symmetry, but no perpendicular symmetry elements (planes or axes). This

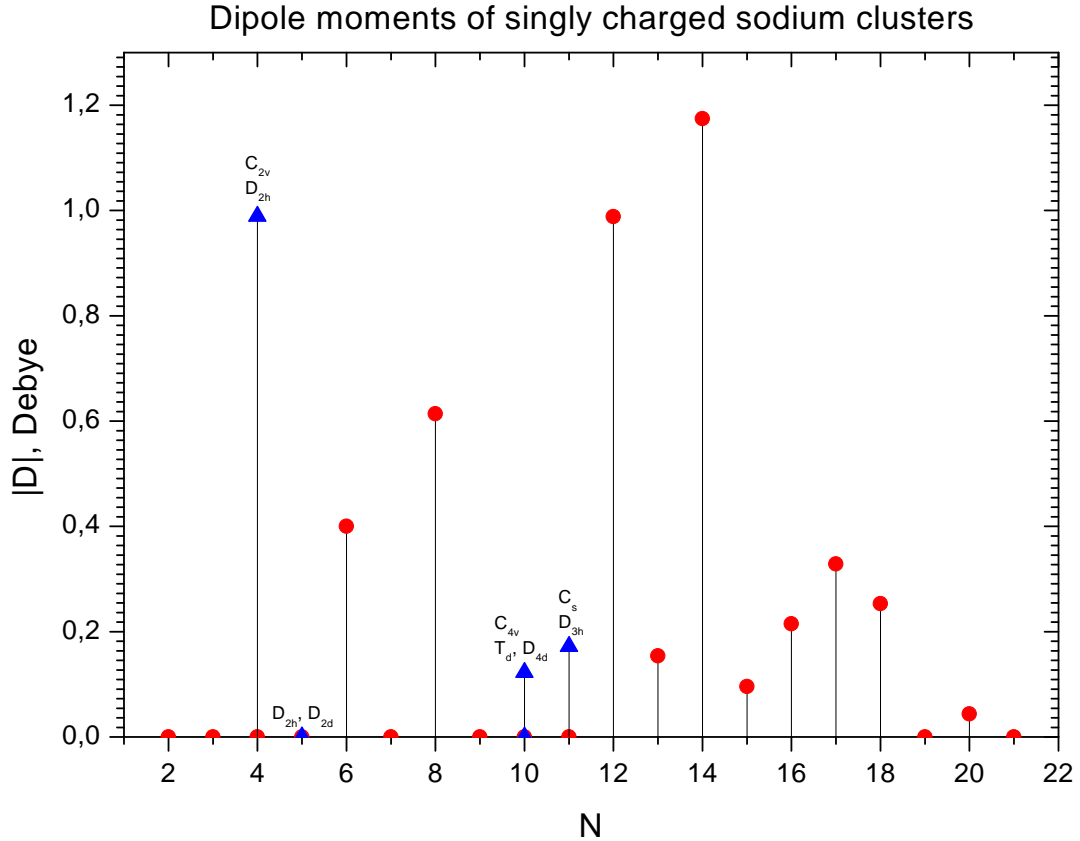


**Figure 11.** Dipole moments for the optimized singly charged sodium clusters as a function of cluster size calculated by the *B3LYP* method. For some clusters, more than one isomer has been considered. In these cases, labels indicate the point symmetry group of corresponding isomers. Geometries of the optimized clusters one can find in figure 2.

rule remains correct even for the  $Na_{20}$  cluster isomer with the symmetry  $C_{2v}$ , which has the closed shell configuration  $1s^2 1p^6 1d^{10} 2s^2$  of delocalised electrons according to the jellium model. Geometries of the cluster ions differ significantly from the geometries of the corresponding neutral clusters, but the rule formulated above on the appearance of the cluster dipole moments remain valid in this case also as it is clear from figure 11.

The principal values of the quadrupole moments tensor for the optimized neutral and singly charged clusters are presented in figures 12 and 13 respectively. For clusters with an axis of symmetry, this axis has been chosen as z-axis of the coordinate system, in which the calculation of the quadrupole moments has been performed. The quadrupole moment tensor is defined as an average value of the following operator:

$$Q_{ij} = \sum q(3x_i x_j - \delta_{ij} r^2) \quad (21)$$

Here, the summation is performed over all electronic and ionic charges in the cluster.

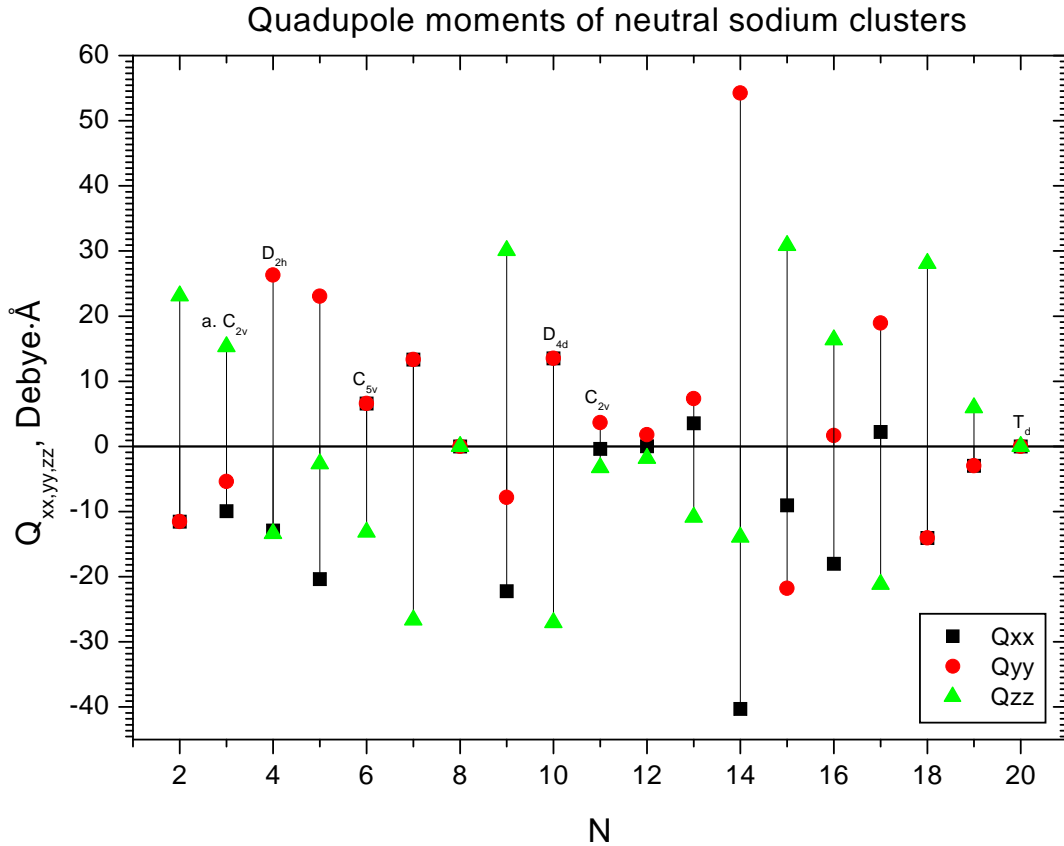


**Figure 12.** The principal values of quadrupole moment tensor for the optimized neutral sodium clusters as a function of cluster size calculated by the *B3LYP* method. Squares, circles and triangles represent the  $Q_{xx}$ ,  $Q_{yy}$  and  $Q_{zz}$  tensor principal values respectively. For some clusters, more than one isomer has been considered. In these cases, labels indicate the point symmetry group of corresponding isomers. Geometries of the optimized clusters one can find in figure 1.

Note that the trace of the tensor  $Q_{ij}$  is equal to zero.

The ionic part of  $Q_{ij}$  can be expressed via the components of the tensor  $R_{ij}$  discussed in section 3.1. Note that the knowledge of  $Q_{ij}$  and  $R_{ij}$  allows one to construct easily the tensor analogous to  $R_{ij}$ , but for electrons. This might be useful for the analysis of deformations of electron density distribution in a cluster.

The quadrupole moment tensor can be expressed via the tensor  $\tilde{Q}_{ij} = \langle \sum q x_i x_j \rangle$ , characterising the averaged dimensions of the total charge distribution. Here, brackets mean averaging over the electronic charge distribution. The principal values of the tensor  $\tilde{Q}_{ij}$  should be negative at least for neutral clusters, because electron density is spilled out of the cluster, which makes its distribution a little broader than the distribution of ions. The similar situation takes place for cluster ions, but in this case there is non-compensated positive charge in the system, which brings certain positive contribution

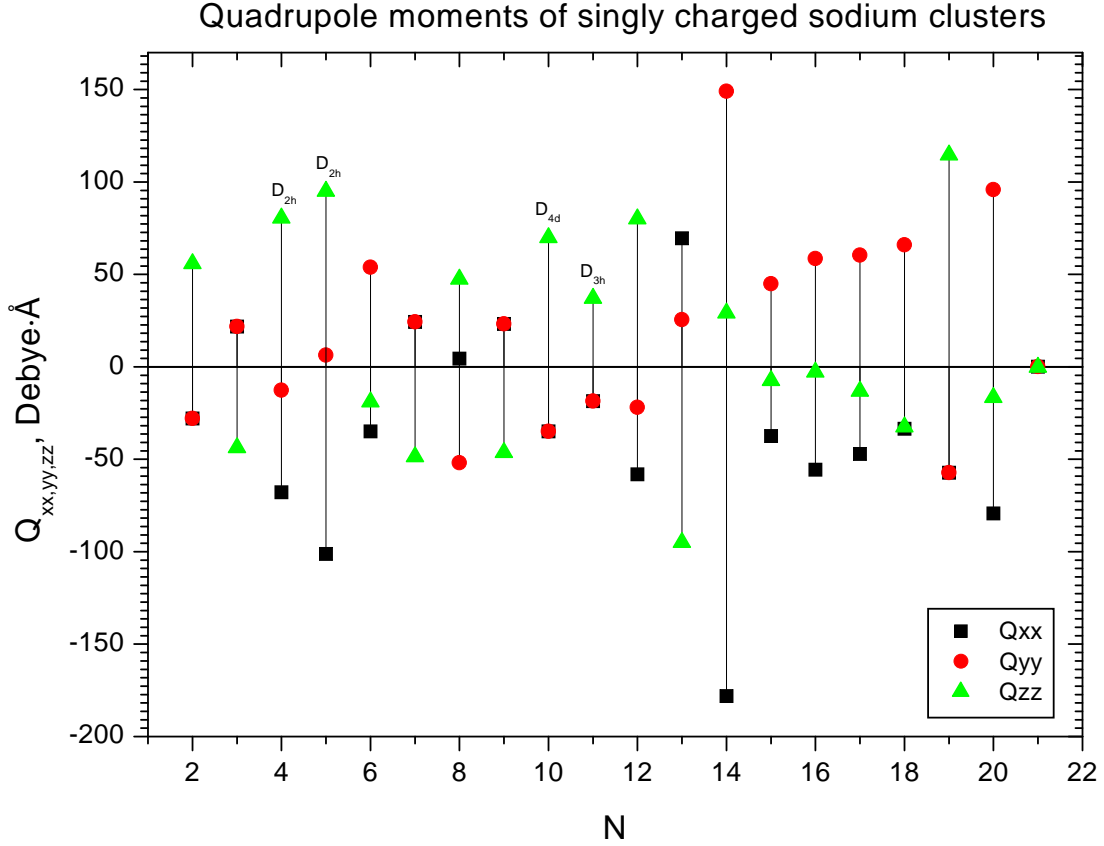


**Figure 13.** The principal values of quadrupole moment tensor for the optimized singly charged sodium clusters as a function of cluster size calculated by the *B3LYP* method. Squares, circles and triangles represent the  $Q_{xx}$ ,  $Q_{yy}$  and  $Q_{zz}$  tensor principal values respectively. For some clusters, more than one isomer has been considered. In these cases, labels indicate the point symmetry group of corresponding isomers. Geometries of the optimized clusters one can find in figure 2.

to  $\tilde{Q}_{ij}$  and makes the principal values of  $\tilde{Q}_{ij}$  positive in some cases.

The numerical analysis performed in this work shows that for neutral sodium clusters the principal values of  $\tilde{Q}_{ij}$  are always negative, while for the small cluster ions:  $Na_2^+$ ,  $Na_3^+$  and  $Na_4^+$  ( $C_{2v}$ ), some of the principal values are positive.

The principle values of the quadrupole moment tensor characterize the distortion of the total cluster charge distribution. Indeed, figure 12 shows that the  $Na_8$  and  $Na_{20}$  tetrahedron group isomers have the zero quadrupole moments, which reflect the closeness to sphericity of the magic clusters. Our calculations demonstrate that for some open shell clusters like  $Na_{11}$  and  $Na_{12}$  the quadrupole moments turn out to be rather small, although the ionic charge distribution in these clusters has the prominent deformation as it is clear from figures 1 and 5. The small quadrupole moments in these clusters is the result of compensation of the electron and ion components of  $Q_{ij}$ .

The quadrupole moments diagram allows one to make some conclusions on the type of the shape of the total charge distribution in a cluster. The averaged dimensions of the cluster total charge distribution in x-, y- and z- directions can be characterized by quantities  $Q_z^{\parallel} = \tilde{Q}_{zz} = \langle \sum ez^2 \rangle$ ,  $Q_x^{\perp} = \tilde{Q}_{xx} = \langle \sum ex^2 \rangle$  and  $Q_y^{\perp} = \tilde{Q}_{yy} = \langle \sum ey^2 \rangle$ . Here, the summation is performed over all electrons and ions in the cluster and brackets mean averaging. These quantities are connected with the quadrupole moments tensor defined in (21). Indeed, in both the prolate and oblate cases, when  $Q_x^{\perp} = Q_y^{\perp} = Q^{\perp}$  and  $Q_z^{\parallel} = Q^{\parallel}$ , the principal values of the tensor  $Q_{ij}$  read as

$$\begin{aligned} Q_{zz} &= 2(Q^{\parallel} - Q^{\perp}) \\ Q_{xx} &= (Q^{\perp} - Q^{\parallel}) = -\frac{Q_{zz}}{2} \\ Q_{yy} &= Q_{xx} = -\frac{Q_{zz}}{2} \end{aligned} \tag{22}$$

These equations define the important relationships between the principal values of the quadrupole moments tensor in the oblate and prolate cases and help understanding the quadrupole moments diagrams shown in figures 12 and 13.

Equations (22) show that the sign of the principal values  $Q_{xx}$ ,  $Q_{yy}$  and  $Q_{zz}$  depends on the relative value of  $Q^{\parallel}$  and  $Q^{\perp}$ . With the use of equations (22) and the cluster quadrupole moment diagrams shown in figures 12 and 13, one can easily analyse the total charge distribution of the clusters shown in figures 1 and 2. Note that conclusions made on the shape of the total charge distribution and the shape of ionic component (see figures 5 and 6) sometimes differ significantly one from another for some clusters. For example, the ionic charge distribution in the  $Na_{12}$  cluster has a prolate shape, while the total charge distribution is oblate.

The quadrupole moments of singly charged sodium clusters differ substantially from those for the corresponding neutral ones. The excessive positive charge leads to the rearrangement of the cluster structure and to the appearance of the quadrupole moment in the cluster ions like  $Na_8^+$  and  $Na_{20}^+$ . Although, the electron exchange-correlation force in a cluster turns out to be insufficient to change the cluster geometry so significantly to make the magic cluster ion  $Na_9^+$ , having the closed shell electronic structure of delocalised electron, spherical-like without quadrupole moment. Instead,  $Na_9^+$  remains a noticeable deformation.

Let us now discuss the idea for which the cluster multipole moments play the crucial role and consider the possibility of the cluster isomers separation by placing the mass selected cluster beam in the inhomogeneous external field. As we have seen from the calculations presented above, different cluster isomers of the same mass often possess different structure and as a result of that different multipole moments (dipole or quadrupole). However, such cluster isomers are indistinguishable in the nowadays experiments with mass selected cluster beams. They can nevertheless be separated if one puts the mass selected cluster beam in the inhomogeneous external field. Let us

estimate this effect for the characteristic values of the dipole and quadrupole moments calculated above.

From the dipole moments diagrams shown in figures 10 and 11 one can conclude that the difference in dipole moments for some cluster isomers can be as large as  $1Debye$  and for the quadrupole often it is about  $40Debye\cdot\text{\AA}$  or even larger. The force acting on the cluster with the dipole moment  $\mathbf{D}$  in an external inhomogeneous electric field  $\mathbf{E}(\mathbf{r})$  is equal to [65]

$$\mathbf{F}^D(\mathbf{r}) = \nabla\{\mathbf{D} \cdot \mathbf{E}(\mathbf{r})\}. \quad (23)$$

The components of the force acting on the cluster with quadrupole moment  $Q_{ij}$  is as follows [65]

$$F_i^Q(\mathbf{r}) = \nabla_i\left\{\frac{Q_{jk}}{6}\nabla_j E_k(\mathbf{r})\right\}. \quad (24)$$

Here, the summation is assumed over the repeated indices  $j$  and  $k$  of the vector and tensor components in the right hand side of (24).

Let us introduce the time period  $\tau$  during which the cluster beam passes the inhomogeneous electric field. One can estimate the distance  $\Delta$  on which isomers will be separated during this period of time as  $\Delta \sim F\tau^2/2M$ , where  $M$  is the mass of the isomer considered and  $F$  is the force acting on either the dipole (see (23)) or quadrupole (see (24)) moment of the cluster. Substituting in these equations the characteristic values for the dipole and quadrupole moments, assuming that the inhomogeneity of the electric field is about  $\nabla E \sim 5 \cdot 10^3 V/cm^2$ , one derives from (23) (24) that during the period  $\tau \sim 10^{-3}s$  the isomers with  $N = 3$  and  $\delta D \sim 1Debye$  become separated on  $\Delta \sim 0.7mm$  and that  $\Delta \sim 2.8mm$  for  $\delta Q \sim 40Debye\cdot\text{\AA}$ ,  $\tau \sim 10s$ ,  $N = 5$  and no dipole moment.

These estimates demonstrate that one can create significant separation distances for reasonably short periods of time with the electric field strengths and their gradients achievable in laboratory conditions. The experiments with mass selected and isomer separated cluster beams could provide the most accurate information on the structure and properties of atomic clusters.

### 3.5. Polarizabilities

We have calculated the polarizabilities for the optimized neutral sodium clusters (see figure 1) as a function of cluster size. Results of this calculation are shown in figure 14. In this figure, we also plot experimental points from [21]. Calculation of the polarizabilities has been performed by the *B3LYP* method. Figure 14 demonstrates quite reasonable agreement of the *B3LYP* results with the experimental data.

In figure 14 we also compare the polarizabilities calculated in our work with those derived by other theoretical methods [19, 32]. This figure demonstrates a satisfactory agreement of the results of different approaches with each other and with the experimental data. This comparison is quite important, because in our work as well as in [19] the polarizabilities have been calculated using all electron *ab initio* approach, while in [32] they were obtained with the use of pseudopotentials. Note that our points

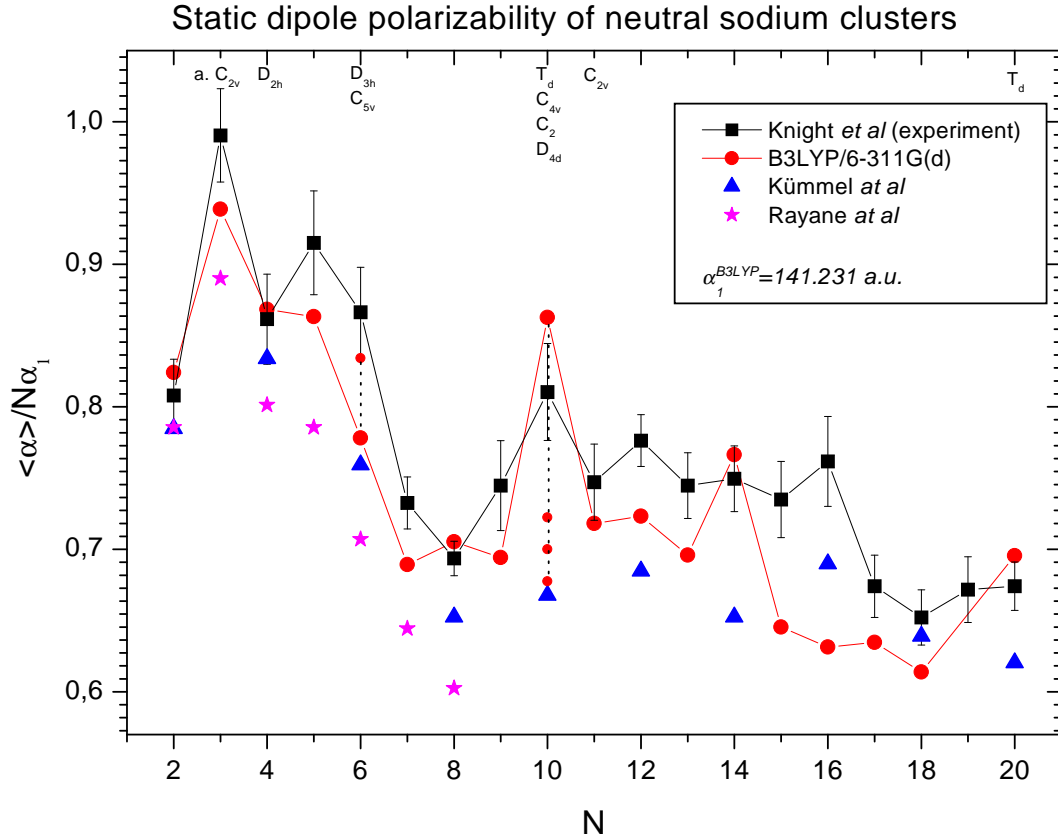


**Figure 14.** Static mean polarizability per atom for neutral sodium clusters normalized to the polarizability of a single sodium atom. Circles show the results derived in this work by the *B3LYP* method. For some clusters, more than one isomer has been considered. In these cases, labels indicate the point symmetry group of corresponding isomers. Stars and triangles represent the polarizabilities calculated in [19] and [32] respectively. Squares are the experimental values taken from [21].

are closer to the experimental values than those from [19], in spite of the fact that both calculations have been performed on the basis of the density functional theory. The difference between the two schemes of calculation arise in the form of the density functional and the employed set of the basis functions. In [19], the so-called Perdew-Wang-91 density functional [62] was used, while we applied its *B3LYP* form.

Let us also compare the polarizabilities for the  $Na_8$  and  $Na_{20}$  clusters calculated in the random phase approximation with exchange in the spherical jellium model,  $\alpha_{Na_8} = 755a.u.$  and  $\alpha_{Na_{20}} = 1808a.u.$  [66], with our results:  $\alpha_{Na_8} = 797a.u.$  and  $\alpha_{Na_{20}} = 1964a.u.$  The closeness of the values show that the detailed ionic core structure does not influence much the value of the clusters polarizabilities. This comparison shows that the jellium model turns out to be quite a reasonable approximation.

Figure 14 shows that the disagreement between theoretical and experimental points

is not always less than the experimental error bars. Such a disagreement might indicate that for certain  $N$  there have been experimentally detected cluster isomers other than those calculated in our work. For example, the calculated value  $\alpha_{Na_6}^{C_{5v}} = 659a.u.$  lies beyond the experimental error bars, while  $\alpha_{Na_6}^{D_{3h}} = 706.876a.u.$  is within the range of the experimental error.

Note that the polarizabilities of clusters  $Na_8$ ,  $Na_{10}$  and  $Na_{20}$ , possessing the  $T_d$  point symmetry group, surpass a little the corresponding experimental values, being quite close to them. For the  $Na_8$  and  $Na_{10}$  clusters, the disagreement of the theoretical and experimental values is within the range of the experimental error. The similar situation occurs for the  $Na_{14}$  cluster, characterized by the  $C_{2v}$  point symmetry group. This cluster likely belongs to the cluster chain leading to the formation of the tetrahedron  $Na_{20}$  cluster from the tetrahedron  $Na_8$  one (see our discussion in section 3.1). Such a situation allows us to assume that the polarizabilities of other clusters of this chain, which we have not analyzed in this paper, because they are energetically not favorable, will be also quite close to the experiment.

### 3.6. Normal vibration modes

Using the *B3LYP* method, we have calculated the normal vibration frequencies for the optimized neutral sodium clusters. The results of this calculation are shown in figure 15. In this figure, we indicate the point symmetry group for those clusters for which more than one cluster isomer has been considered (see figure 1). Numerous frequencies shown in figure 15 are degenerate or nearly degenerate. This explains why the total number of frequencies for most of clusters is less than the number of vibrational degrees of freedom available in the system. In the more symmetric clusters, like  $Na_7$ ,  $Na_8$ ,  $Na_{10}$  or  $Na_{20}$ , the rate of generacy of the normal vibration modes is higher.

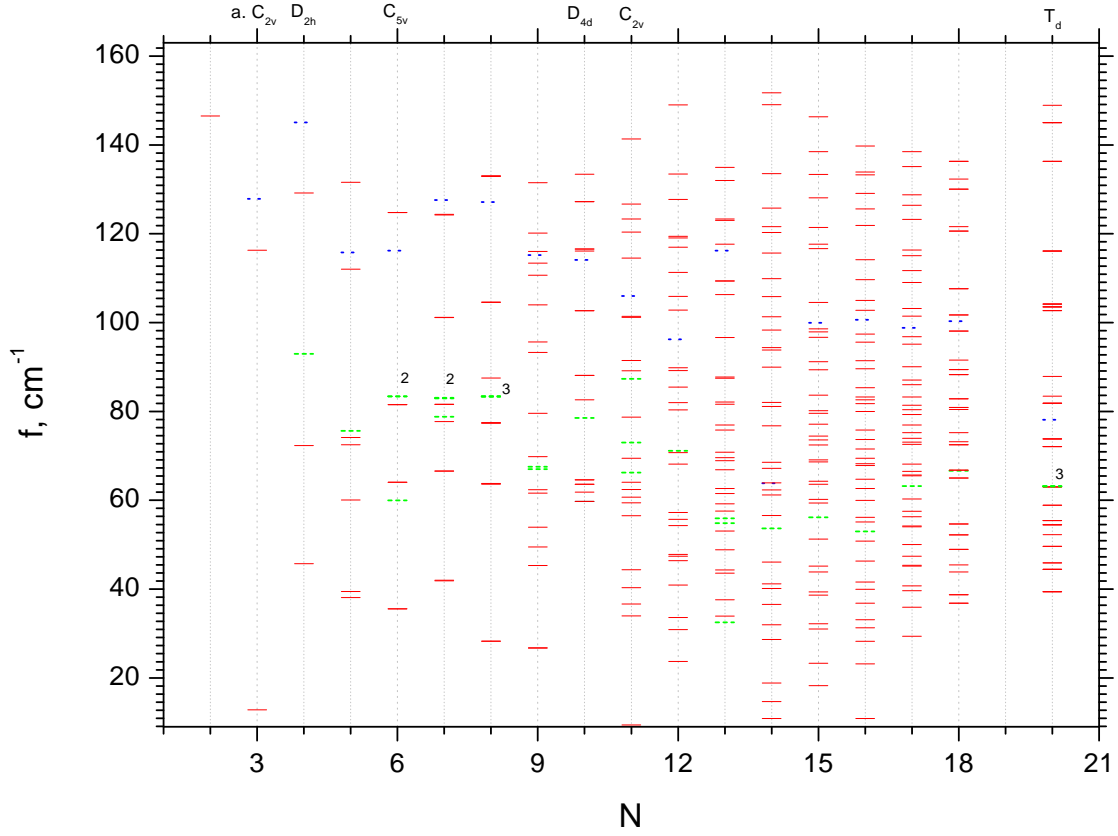


**Figure 15.** Normal vibration frequencies calculated by the *B3LYP* method for the neutral sodium clusters with  $N \leq 20$ . For each cluster we mark the breathing mode in the spectrum by dotted line and the surface quadrupole vibration modes by dashed lines. The number near some of the lines indicate the degeneracy of the corresponding mode. Note that we make this only for quadrupole surface vibration modes.

Knowledge of normal vibration modes and their frequencies is important for physical understanding and quantitative description of the relaxation of electron plasmon excitations in metal clusters [42]. One can visualize normal vibration modes, showing the directions and amplitudes of the atoms displacements by corresponding vectors. Since it is difficult to show all such pictures in this paper due to their large number. We focus instead only on the two types of modes breathing and quadrupole surface vibration modes. Namely these modes have been considered in [42] within the dynamical jellium model [41] for the treatment of the electron-phonon coupling in the spherical metal clusters  $Na_{20}$ ,  $Na_{40}$  and  $Na_{92}$ .

In this paper, we discuss the appearance of these specific vibration modes in a cluster system and compare their frequencies with the predictions made in [42] on the basis of the jellium model. For this purpose, we have analysed all calculated vibration

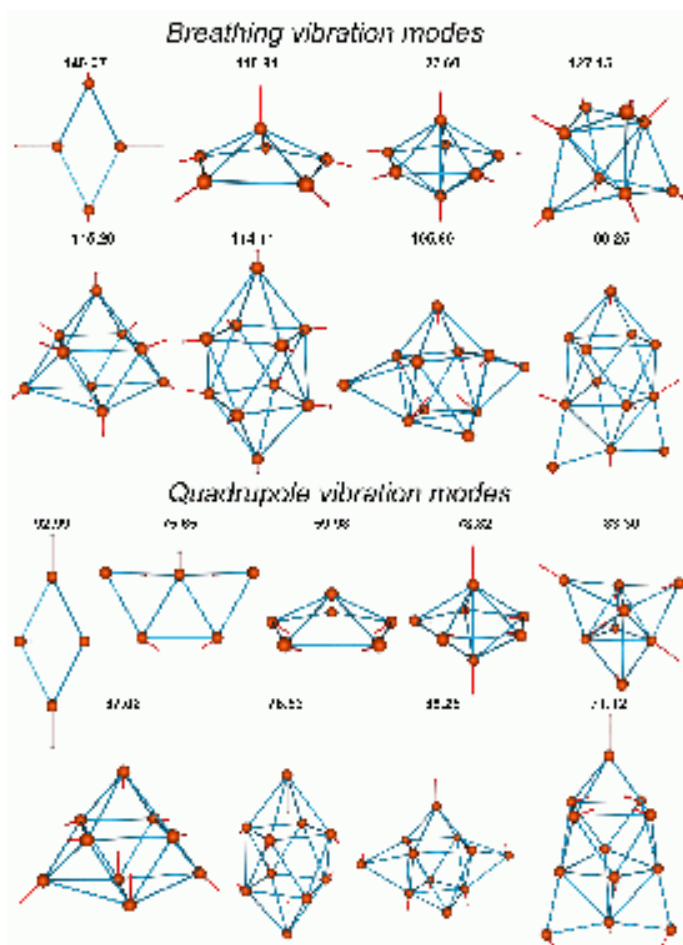


**Figure 16.** Surface and volume vibration modes for the selected neutral sodium clusters. Number near each cluster image indicates the frequency of the corresponding normal vibration mode. The values are given in  $cm^{-1}$ .

modes and identified the breathing and three quadrupole vibrations for each cluster. In figure 16, we present images of the breathing and quadrupole vibration modes for some clusters to illustrate the way, how the identification of the modes has been performed. This figure shows that the identification made is definite enough.

The results of this analysis are shown in figure 15, where for each cluster we mark the breathing mode in the spectrum by dotted line and the surface quadrupole vibration modes by dashed lines. The number near some of the lines indicate the degeneracy of the corresponding modes. Note that we make this only for quadrupole surface vibration modes. The degeneracy rate and the number of quadrupole surface vibration modes can be easily understood with the help of the cluster images shown in figure 1. This figure shows that the prototype of the breathing mode exists already in the  $Na_3$  and  $Na_4$  clusters. For the  $Na_4$  cluster, one can identify the quadrupole surface vibration mode, although it is meaningful to discuss surface vibrations only for the  $Na_6$  cluster and larger. Figure 15 shows the frequencies of the breathing and surface vibration

modes decrease systematically with increasing cluster size, although this decrease has numerous irregularities, particularly for the clusters with  $N < 8$ . The frequency of the breathing mode decreases faster with the growth of  $N$  than the frequency of the quadrupole surface vibration mode.

Let us compare the calculated frequencies of the breathing and surface vibration modes with the predictions of the jellium model. In [42], it was shown that the breathing vibration mode frequencies calculated for the spherical  $Na_{20}$ ,  $Na_{40}$  and  $Na_{92}$  respectively within the framework of the dynamical jellium model are quite close to the values derived from the phonon dispersion law for metals [67]

$$\Omega^2 = \frac{3v_F^2 k^2}{M_{Na}(9 + k^2 v_F^2 r_0^3)}, \quad (25)$$

where  $M_{Na} = 4.2 \cdot 10^4$  is the mass of sodium atom,  $v_F = (9\pi/4)^{1/3}/r_0$  is the velocity of cluster electrons on the Fermi surface,  $r_0$  is the Wigner-Seitz radius. In the long wave limit, equation (25) reduces to the Bohm-Staver formula for the velocity of sound,  $d\Omega/dk = v_F/\sqrt{3M_{Na}} \approx 3 \cdot 10^5 \text{ cm/s}$ . This number is quite close to the real value of the velocity of sound in the bulk sodium:  $3.2 \cdot 10^5 \text{ cm/s}$ .

Using the dispersion law (25), we estimate the breathing mode frequencies for the magic  $Na_8$  and  $Na_{20}$  clusters. The results of this calculation are as follows  $\Omega_{Na_8} = 104.09 \text{ cm}^{-1}$ ,  $\Omega_{Na_{20}} = 80.49 \text{ cm}^{-1}$ . In this calculation we have used  $r_0 = 4$ .

The frequency values obtained from (25) are close to those presented in figure 15,  $\Omega_{Na_8} = 127.15 \text{ cm}^{-1}$ ,  $\Omega_{Na_{20}} = 78.11 \text{ cm}^{-1}$ . The agreement of the frequencies is rather good for the  $Na_{20}$  cluster case. For  $Na_8$ , the agreement is reasonable, but not as good as for  $Na_{20}$ . Some disagreement arises due to the fact that the Wigner-Seitz radius for the  $Na_8$  cluster is about 10% smaller than its bulk value. Indeed, substituting  $r_0 = 3.6$  in (25) one derives  $\Omega_{Na_8} = 127.10 \text{ cm}^{-1}$ , which is in the nearly perfect agreement with the *ab initio* result. The decrease of the Wigner-Seitz radius can be easily understood from the analysis of the cluster geometry shown in figure 1.

Now let us compare the quadrupole surface vibration mode frequencies calculated in our paper (see figure 15) with those following from the dynamical jellium model. According to [42], the quadrupole surface vibration frequencies,  $\Omega_2$ , for the spherical  $Na_{20}$ ,  $Na_{40}$  and  $Na_{92}$  clusters are equal to  $56.48 \text{ cm}^{-1}$ ,  $48.41 \text{ cm}^{-1}$  and  $32.28 \text{ cm}^{-1}$ , respectively. The value of the quadrupole surface vibration frequency for the  $Na_{20}$  cluster calculated in the present work is equal to  $63.15 \text{ cm}^{-1}$ , which is rather close to the value predicted in [42].

The values of the quadrupole surface vibration frequencies calculated for  $Na_{20}$ ,  $Na_{40}$  and  $Na_{92}$  show relatively slow decrease with the growth cluster size. Extrapolating these values towards smaller cluster sizes, we derive frequency values, which are consistent with those shown in figure 15. This comparison demonstrates that the jellium model calculation of the surface vibration frequencies is in a reasonable agreement with the more accurate *ab initio* many-body theory.

The comparison of the jellium model results with those derived by the more accurate

*ab initio* many-body theory is important, because it forms theoretical background for the jellium model calculations in larger cluster systems, for which *ab initio* methods are hardly possible. The comparison with the jellium model, which we performed in this paper, can be extended towards larger cluster sizes and other collective modes of ions motion.

#### 4. Conclusion

In this paper we have calculated the optimized structure and various characteristics of sodium clusters consisting of up to 20 atoms. We have used three different methods: *B3LYP*, *MP<sub>4</sub>* and *HF*. It was demonstrated that the first two methods due to accounting for many-electron correlations provide much better agreement with the available experimental data and theoretical results based of the configuration interaction method as compared to that for the Hartree-Fock approximation. This was checked for various cluster characteristics: cluster geometries, binding energies per atom and the ionization potentials.

We have also calculated and analyzed the dependence of the ionic component and total quadrupole moments of sodium clusters as a function of their size. It was demonstrated that the cluster shapes characterized by the quadrupole moments are in a reasonable agreement with the predictions of the jellium model and the results of the experimental observations.

We have determined the normal vibration modes and their frequencies for a number of clusters and demonstrated their qualitative agreement with the predictions based on the jellium model.

The results of this work can be extended in various directions. One can use the similar methods to study structure and properties of various types of clusters. It is interesting to extend calculations towards larger cluster sizes and perform more comparison with the results following from the jellium model and other simplified theories, based either on pseudopotentials or effective interatomic potentials. A lot of novel problems arise, when considering collisions and electron excitations in the clusters with the optimized geometries. These and many more other problems on atomic cluster physics can be tackled with the use of methods considered in our work.

#### 5. Acknowledgements

The authors acknowledge support from the INTAS, the Volkswagen Foundation, the Alexander von Humboldt Foundation and DAAD.

#### References

- [1] Knight W D, Clemenger K, de Heer W A , Saunders W A , Chou M Y and Cohen M L 1984 *Phys. Rev. Lett.* **52** 2141
- [2] Bréchnignac C, Cahuzac Ph, Carlier F, Leygnier J 1989 *Chem. Phys. Lett.* **164** 433

- [3] Selby K, Vollmer M, Masui J, Kresin V, de Heer W A, and Knight W D 1989 *Phys. Rev. B* **40** 5417
- [4] Selby K, Kresin V, Masui J, Vollmer M, de Heer W A, Scheidemann A, Knight W D 1991 *Phys. Rev. B* **43** 4565
- [5] Bertsch G F, Bulcac A, Tomanek D, Wang Y 1992 *Phys. Rev. Lett.* **67** 1991
- [6] Hertel I V, Steger H, de Vries J, Weisser B, Menzel C, Kamke B and Kamke W 1992 *Phys. Rev. Lett* **68** 784
- [7] Herlert A, Krückeberg S, Schweikhard L, Vogel M, Walther C 1999 *Physica Scripta T* **80** 200
- [8] de Heer W A 1993 *Rev. Mod. Phys.* **65** 611
- [9] Brack M 1993 *Rev. Mod. Phys.* **65** 677
- [10] Bréchnignac C, Connerade J P 1994 *J.Phys.B:At.Mol.Opt.Phys.* **27** 3795
- [11] Haberland H (ed.) 1994 *Clusters of Atoms and Molecules, Theory, Experiment and Clusters of Atoms* (Springer Series in Chemical Physics **52**) (Berlin: Springer)
- [12] Näher U, Bjørnholm S, Frauendorf S, Garcias F and Guet C 1997 *Physics Reports* **285** 245
- [13] Ekardt W (ed.) 1999 *Metal Clusters* (New York: Wiley)
- [14] Proceedings of the Les Houches 2000 Summer School *Atomic Clusters and Nanoparticles* July 2000 (Les Houches, France) (to be published in EDP Sciences and Springer Verlag)
- [15] Boustani I, Pewestorf W, Fantucci P, Bonačić-Kotecký V, Kotecký J 1987 *Phys. Rev. B* **35** 9437
- [16] Bonačić-Kotecký V, Fantucci P, Kotecký J 1988 *Phys. Rev. B* **37** 4369
- [17] Boustani I, Kotecký J 1988 *J. Chem. Phys.* **88** 5657
- [18] Bonačić-Kotecký V, Boustani I, Guest M F, Kotecký J 1988 *J. Chem. Phys.* **89** 4861
- [19] Rayane D et al. 1999 *Eur. Phys. J.* **D9** 243
- [20] Akeby H, Panas I, Petterson L G M, Siegbahn P, Wahlgreen U 1990 *J. Chem. Phys.* **94** 5471
- [21] Knight W D, Clemenger K, de Heer W A, Saunders W A 1985 *Phys. Rev. B* **31** 2539
- [22] Bréchnignac C, Cahuzac Ph, Leygnier J and Weiner J 1492 *J. Chem. Phys.* **90** 1492
- [23] Bréchnignac C, Cahuzac Ph, Carlier F, de Frutos M and Leygnier J 1990 *J. Chem. Phys.* **93** 7449
- [24] Bréchnignac C, Cahuzac Ph, Carlier F, Leygnier J and Sarfati A 1991 *Phys. Rev. B* **44** 11386
- [25] de Heer W A, Selby K, Kresin V, Masui J, Vollmer, Chatelain A and Knight W D 1987 *Phys. Rev. Lett.* **59** 1805
- [26] Martins J L, Buttet J and Car R 1985 *Phys. Rev. B* **31** 1804
- [27] Spiegelmann F, Poteau R, Montag B, Reinhard P-G, 1998 *Physics Letters* **A242** 163
- [28] Nogueira F, Martins J L and Fiolhais C, 1999 *Eur. Phys. J.* **D9** 229
- [29] Gutié rrez R, Grossmann F, Knospe O, Schmidt R 2001 *Phys. Rev.* **A64** 013202
- [30] Blundell S A, Guet C, Rajendra R Zope 2000 *Phys. Rev. Lett.* **84** 4826
- [31] Kronik L, Vasiliev I and Chelikowsky J R 2000 *Phys. Rev.* **B62** 9992
- [32] Kü mmel S, Berkus T, Reinhard P-G and Brack M 2000 *Eur. Phys. J.* **D11** 239
- [33] Kü mmel S, Akola J and Manninen M 2000 *Phys. Rev. Lett.* **84** 3827
- [34] Martins J L, Car R and Buttet J 1981 *Surf. Sci.* **106** 265
- [35] Hintermann A and Manninen M 1983 *Phys. Rev. B* **27** 7262
- [36] Ekardt W 1984 *Phys. Rev. B* **29** 1558
- [37] Ekardt W 1985 *Phys. Rev. B* **32** 1961
- [38] Guet C and Johnson W R 1992 *Phys. Rev. B* **45** 283
- [39] Ivanov V K, Ipatov A N, Kharchenko V A, Zhizhin M L 1993 *Pis'ma JETPh* (in Russian) **58** 649; 1994 *Phys. Rev. A* **50** 1459
- [40] Lyalin A G, Semenov S K, Solov'yov A V, Cherepkov N A and Greiner W 2000 *J. Phys. B: At. Mol. Opt. Phys.* **33** 3653
- [41] Gerchikov L G, Solov'yov A V, Greiner W 1999 *International Journal of Modern Physics E* **8** 289
- [42] Gerchikov L G, Ipatov A N, Solov'yov A V and Greiner W 2000 *J. Phys. B: At. Mol. Opt. Phys.* **33** 4905-4926
- [43] Ivanov V K 1996 *Correlations in Clusters and Related Systems* ed. J-P Connerade (Singapore: World Scientific) pp 73-91

- [44] Bertsch G F, Bulgac A, Tomanek D and Wang Y 1991 *Phys. Rev. Lett.* **67** 2690
- [45] Ivanov V K, Kashenock G Yu, Polozkov R G, Solov'yov A V 2001 *accepted as Letter to the Editor in J. Phys. B: At. Mol. Opt. Phys.*
- [46] Gerchikov L G, Connerade J P, Solov'yov A V and Greiner W 1997 *J. Phys. B: At. Mol. Opt. Phys.* **30** 4133-4161
- [47] Gerchikov L G, Efimov P V, Mikoushkin V M and Solov'yov A V 1998 *Phys. Rev. Lett.* **81** 2707-2710.
- [48] Gerchikov L G, Ipatov A N and Solov'yov A V 1997 *J. Phys. B: At. Mol. Opt. Phys.* **30** 5939-59359
- [49] Gerchikov L G, Ipatov A N, Solov'yov A V and Greiner W 1998 *J. Phys. B: At. Mol. Opt. Phys.* **31** 3065-3077
- [50] Gerchikov L G, Ipatov A N, Polozkov R G and Solov'yov A V 2000 *Phys. Rev. A* **62** 043201
- [51] Connerade J P, Gerchikov L G, Ipatov A N and Solov'yov A V 1998 *J. Phys. B: At. Mol. Opt. Phys.* **31** L27-L34
- [52] Connerade J P, Gerchikov L G, Ipatov A N and Solov'yov A V 1999 *J. Phys. B: At. Mol. Opt. Phys.* **32** 877-894
- [53] Gerchikov L G and Solov'yov A V 1997 *Z. Phys. D: Atoms, Molecules, Clusters* **42** 279-287
- [54] Gerchikov L G, Ipatov A N and Solov'yov A V 1998 *J. Phys. B: At. Mol. Opt. Phys.* **31** 2331-2341
- [55] Solov'yov A V, "Electron scattering on metal clusters and fullerenes", in Proceedings of the Les Houches 2000 Summer School *Atomic Clusters and Nanoparticles* July 2000 (Les Houches, France) (to be published in EDP Sciences and Springer Verlag)
- [56] Frisch M J, Trucks G W and *et al* 1998  
*Gaussian 98* (Revision A.9) Gaussian Inc. Pittsburgh PA
- [57] Lindgren I and Morrison J 1986 *Atomic Many-Body Theory* (Springer-Verlag, New York Heidelberg Berlin).
- [58] James B. Foresman and Æleen Frisch *Exploring Chemistry with Electronic Structure Methods* 1996 (Pittsburgh, PA: Gaussian Inc)
- [59] Møller C and Plesset M S 1934 *Phys. Rev.* **46**, 618
- [60] Landau L D and Lifshitz E M 1965 *Quantum Mechanics* (London: Pergamon)
- [61] Becke A D 1988 *Phys. Rev. A* **38**, 30098
- [62] Burke K, Perdew J P and Wang Y, in *Electronic Density Functional Theory: Recent Progress and New Directions*, Ed. Dobson J F, Vignale G and Das M P 1998 (Plenum)
- [63] Lee C, Yang W and Parr R G 1988 "a functional of the electron density", *Phys. Rev. B* **37** 785
- [64] Vosko S H, Wilk L and Nusair M 1980 "critical analysis", *Canadian J. Phys.* **58** 1200
- [65] Landau L D and Lifshitz E M 1959 *The Classical Theory of Fields* (London: Pergamon)
- [66] Madjet M, Guet C and Johnson W R 1995 *Phys. Rev. A* **51** 1327
- [67] Kittel C 1967 *Introduction to Solid state Physics* (London: John Wiley & Sons)

## Appendix A. Tables

In Appendix, we present tables of the essential cluster characteristics. The binding energies per atom for neutral and singly charged clusters are compiled in tables A1 and A2. The principal values of the quadrupole moment tensor for neutral and singly charged clusters are presented in tables A3 and A4.

N	Symmetry	$E_N$ (a.u.)			
		HF/6-311G(d)	MP4/6-311G(d,p)	B3LYP/6-311G(d)	Ref: [16]
1		-161.8459	-161.8459	-162.2866	-
2	$D_{\infty h}$	-323.6911	-323.7149	-324.5999	-323.3176
3	$D_{\infty h}$	-485.5405	-485.5626	-486.8963	-
	$a.C_{2v}$	-485.5403	-485.5653	-486.8960	-484.9729
	$b.C_{2v}$	-485.5385	-485.5656	-486.8939	-
	$D_{3h}$	-485.5282	-485.5626	-486.8889	-
4	$D_{2h}$	-647.3871	-647.4433	-649.2076	-646.6494
	$D_{4h}$	-647.3897	-	-649.1965	-
5	$C_{2v}$	-809.2518	-809.3008	-811.5164	-808.3174
6	$C_{5v}$	-971.0915	-971.1880	-973.8324	-969.9899
	$D_{3h}$	-971.0998	-971.1872	-973.8344	-989.9884
7	$D_{5h}$	-1132.9462	-1133.0634	-1136.1430	-1131.6610
8	$T_d$	-1294.8015	-1294.9410	-1298.4606	-1293.3395
9	$C_{2v}$	-1456.6466	-	-1460.7597	-
10	$C_2$	-	-	-1623.0758	-
	$D_{4d}$	-	-	-1623.0734	-
	$C_{4v}$	-	-	-1623.0554	-
	$T_d$	-	-	-1623.0530	-
11	$C_{2v}$	-	-	-1785.3737	-
	$C_1$	-	-	-1785.3726	-
12	$C_{2v}$	-	-	-1947.6917	-
13	$C_1$	-	-	-2110.0045	-
14	$C_{2v}$	-	-	-2272.3092	-
15	$C_s$	-	-	-2434.6188	-
16	$C_s$	-	-	-2596.9370	-
17	$C_s$	-	-	-2759.2537	-
18	$C_{5v}$	-	-	-2921.5704	-
19	$D_{5h}$	-	-	-3083.8730	-
20	$T_d$	-	-	-3246.2015	-
	$C_{2v}$	-	-	-3246.1981	-

**Table A1.** In this table we present the total energies of the optimized neutral sodium clusters. Numbers of atoms in clusters are given in the first column. In the second column, the point symmetry groups of clusters are shown. In the next three columns, the cluster total energies derived by the *HF*, *MP<sub>4</sub>* and *B3LYP* methods are compiled. For the sake of comparison, the total energies computed by the *CI* method in [16] are presented in the sixth column.

N	Symmetry	$E_N^+$ (a.u.)		
		HF/6-311G(d)	MP4/6-311G(d,p)	B3LYP/6-311G(d)
1		-161.6642	-161.6642	-162.0874
2	$D_{\infty h}$	-323.5447	-323.5447	-324.4114
3	$D_{3h}$	-485.4084	-485.4322	-486.7457
4	$D_{2h}$	-647.2653	-647.2915	-649.0502
	$C_{2v}$	-647.2681	-647.2919	-649.0489
5	$D_{2h}$	-809.1226	-809.1740	-811.3727
	$D_{2d}$	-	-	-811.3629
6	$C_{2v}$	-970.9749	-971.0364	-973.6742
7	$D_{5h}$	-1132.8278	-1132.9261	-1135.9994
8	$C_{2v}$	-1294.6866	-1294.7863	-1298.3082
9	$D_{3h}$	-1456.5346	-	-1460.6326
10	$D_{4d}$	-	-	-1622.9335
	$C_{4v}$	-	-	-1622.9278
	$T_d$	-	-	-1622.9273
11	$D_{3h}$	-	-	-1785.2509
	$C_s$	-	-	-1785.2455
12	$C_{2v}$	-	-	-1947.5479
13	$C_1$	-	-	-2109.8718
14	$C_{2v}$	-	-	-2272.1654
15	$C_s$	-	-	-2434.4907
16	$C_s$	-	-	-2596.8051
17	$C_s$	-	-	-2759.1222
18	$C_s$	-	-	-2921.4365
19	$D_{5h}$	-	-	-3083.7499
20	$C_{2v}$	-	-	-3246.0655
21	$O_h$	-	-	-3408.3434

**Table A2.** In this table we present the total energies of the optimized singly charged sodium clusters. Numbers of atoms in clusters are given in the first column. In the second column, the point symmetry groups of clusters are shown. In the next three columns, the cluster total energies derived by the *HF*, *MP4* and *B3LYP* methods are compiled.

N	Symmetry	$Q_{xx}$ , (DebyeÅ)	$Q_{yy}$ , (DebyeÅ)	$Q_{zz}$ , (DebyeÅ)
2	$D_{\infty h}$	-11.5622	-11.5622	23.1244
3	$a.C_{2v}$	-9.9300	-5.3883	15.3183
	$b.C_{2v}$	-7.5625	31.0631	-23.5006
	$D_{\infty h}$	-16.3309	-16.3309	32.6618
4	$D_{2h}$	-12.9139	26.2865	-13.3726
	$D_{4h}$	5.1177	5.1177	-10.2354
5	$C_{2v}$	-20.3760	23.0544	-2.6784
6	$C_{5v}$	6.5817	6.5817	-13.1634
	$D_{3h}$	14.4807	14.4807	-28.9614
7	$D_{5h}$	13.3285	13.3285	-26.6570
8	$T_d$	0.0000	0.0000	0.0000
9	$C_{2v}$	-22.2202	-7.8457	30.0659
10	$D_{4d}$	13.5248	13.5248	-27.0496
	$C_2$	31.6087	-15.5561	-16.0526
	$C_{4v}$	-14.6949	-14.6949	29.3898
	$T_d$	0.0000	0.0000	0.0000
11	$C_{2v}$	-0.3816	3.6348	-3.2532
	$C_1$	-18.4455	13.9570	4.48848
12	$C_{2v}$	0.0392	1.7777	-1.8169
13	$C_1$	3.5616	7.3169	-10.8785
14	$C_{2v}$	-40.2978	54.2376	-13.9398
15	$C_s$	-9.0476	-21.7878	30.8354
16	$C_s$	-18.0272	1.6718	16.3554
17	$C_s$	2.2310	18.9437	-21.1747
18	$C_{5v}$	-14.0456	-14.0540	28.0996
19	$D_{5h}$	-2.9626	-2.9626	5.9252
20	$T_d$	0.0000	0.0000	0.0000
	$C_{2v}$	-69.7510	79.8143	-10.0633

**Table A3.** In this table we present the principal values of the quadrupole moment tensor calculated for neutral sodium clusters. The first column shows numbers of atoms in clusters. The second column gives their point symmetry groups. In the last three columns, the principal values  $Q_{xx}$ ,  $Q_{yy}$  and  $Q_{zz}$  are given. They have been computed by the *B3LYP* method.

N	Symmetry	$Q_{xx}$ , (DebyeÅ)	$Q_{yy}$ , (DebyeÅ)	$Q_{zz}$ , (DebyeÅ)
2	$D_{\infty h}$	-27.9109	-27.9109	55.8218
3	$D_{3h}$	21.8547	21.8547	-43.7094
4	$D_{2h}$	-67.8170	-12.6716	80.4886
	$C_{2v}$	-86.4460	-27.4786	113.9246
5	$D_{2h}$	-101.2157	6.2746	94.9411
	$D_{2d}$	-46.6091	-46.6091	93.2182
6	$C_{2v}$	-34.9108	53.8712	-18.9604
7	$D_{5h}$	24.3267	24.3267	-48.6534
8	$C_{2v}$	4.4346	-51.8751	47.4405
9	$D_{3h}$	23.1994	23.1994	-46.3988
10	$D_{4d}$	-34.9547	-34.9547	69.9094
	$C_{4v}$	-3.5448	-3.5448	7.0896
	$T_d$	0.0000	0.0000	0.0000
11	$D_{3h}$	-18.5476	-18.5476	37.0952
	$C_s$	19.4836	-10.0197	-9.46382
12	$C_{2v}$	-58.0823	-21.8996	79.9819
13	$C_1$	69.5400	25.4745	-95.0145
14	$C_{2v}$	-178.1183	149.0275	29.0908
15	$C_s$	-37.4527	44.8752	-7.4225
16	$C_s$	-55.6664	58.5058	-2.8394
17	$C_s$	-47.1267	60.3728	-13.2461
18	$C_s$	-33.5207	65.9999	-32.4792
19	$D_{5h}$	-57.3045	-57.3045	114.6090
20	$C_{2v}$	-79.3111	95.8676	-16.5565
21	$O_h$	0.0967	0.0967	-0.1934

**Table A4.** In this table we present the principal values of the quadrupole moment tensor calculated for singly-charged sodium clusters. The first column shows numbers of atoms in clusters. The second column gives their point symmetry groups. In the last three columns, the principal values  $Q_{xx}$ ,  $Q_{yy}$  and  $Q_{zz}$  are given. They have been computed by the *B3LYP* method.